Received: 9 May 2025 | Revised: 21 August 2025 | Accepted: 26 September 2025

DOI: 10.1002/gamm.70009

ORIGINAL ARTICLE

GAMM Mitteilungen

Gradient Crystal Plasticity Modeling of Laminate Microstructures

Claudius Klein | **Thomas Böhlke**

Institute of Engineering Mechanics, Karlsruhe Institute of Technology (KIT), Kaiserstraße 10, Karlsruhe, Germany

Correspondence
Thomas Böhlke, Institute of Engineering Mechanics, Karlsruhe Institute of Technology (KIT), Kaiserstraße 10, 76131 Karlsruhe, Germany.
Email: thomas.boehlke@kit.edu

Abstract

Metallic materials may show an ultra-fine lamellar morphology leading to desirable macroscopic mechanical properties. In this paper, an analytical method for modeling the size-dependent mechanical behavior of material systems with lamellar microstructure is proposed. The main contribution of this manuscript is the combination of the exact elastic localization relations for a periodic laminate having inhomogeneous phases with a gradient plasticity constitutive model. This allows a new formulation of the equations governing the evolution of the plastic deformation as a closed system of equations. The yield functions form a system of integro-differential equations that can be solved analytically. This new framework allows to model the size-dependent mechanical behavior of multiphase lamellar materials where the subdomains are elastoplastic single crystals. This is demonstrated using a two-phase laminate. In addition, bounds for the qualitative distributions of the plastic slip and the back stress are derived using a dimensionless quantity. The kinematic hardening due to the back stress depends on the lamella width and the slip system orientation. The back stress vanishes not only for increasing lamella widths but also in slip systems where the slip plane normal is parallel to the lamination direction.

KEYWORDS

gradient crystal plasticity, laminate microstructures, micro mechanics, size effect

1 | INTRODUCTION

Alloys with lamellar microstructures have excellent mechanical properties making them promising material choices for structural components in modern, high performance engineering applications. They have thus been the subject of numerous experimental and numerical investigations. [30] produced ultra-fine structured steel via chemical patterning with subsequent tests of macroscopic samples achieving ultimate tensile strengths up to 2.1 GPa. The macroscopic compression creep response and microstructural evolution of binary Fe–Al alloys with lamellar microstructures have been studied by [24] and [23], observing inhomogeneous plastic deformation as well as an increase of interface dislocations. Using micropillar compression tests of lamellar TiAl structures, [20, 21] found a significant influence of the lamella width and their orientation relative to the load direction. [15] investigated lamellar structures in high-entropy alloys with two distinct phases, which showed fixed orientation relationships within the same lamellar domain. [16]

identified extensive pile-up of geometrically necessary dislocations near the phase interfaces as the relevant hardening mechanism. The mechanical behavior of lamellar TiAl alloys was investigated numerically by [25] and [26]. Both works model the size-dependency by a Hall-Petch relationship for the critical shear stress in each slip system. Additionally, the slip systems are categorized into three modes of different strength according to [14]. Alternatively, the size-dependent mechanical behavior can be modeled using gradient extended constitutive models [11] with a systematic approach thereof given by [6]. In the context of laminates, [3] studied the influence of different defect energy exponents of the local distributions of the plastic strain, while comparisons with results from discrete dislocations dynamics simulations are given. Analytical approaches of size-dependent plasticity in laminates include the comparison of different nonlocal continuum theories by [28] and [8]. Comparisons of different defect energies are given by [7]. Further works include the study of kinematic hardening during cyclic deformation [33] and the study of size effects by [4] and [2]. Investigations of different grain boundary models, taking slip transmission at the interface into account, have been conducted by [22] and [5]. The analytical investigations of gradient plasticity in lamellar materials are limited in terms of the investigated material systems and load cases. The elastic stiffness is often homogeneous and isotropic while the single slip system is well-aligned with the lamination. For the load case of pure shear, this configuration allows for an analytical solution. However, the generalization to arbitrary lamellar material systems subjected to arbitrary strain rates is not obvious. For classical laminates, that is, without gradient enhancements, a plethora of analytical approaches exist to access the local stress and strain fields, cf. [10, 18] for investigations of the elastic behavior. A more extensive overview, including the plastic behavior, is given by [9]. However, the most general formulation of the stress and strain localizations is given by [12], where, in contrast to previous works, explicit expressions for the local stress and strain fields are derived without the common assumption of piece-wise constant stress and strain fields. This allows for the consideration of in lamination direction spatially inhomogeneous stress and strain fields within the laminate phases using a compact notation.

Outline. This work starts with a brief introduction of the gradient-enhanced rate-independent crystal plasticity model. Next, a general overview is given of the mechanics of laminates, with the focus on locally inhomogeneous fields and the exact strain localization relation. Subsequently, the constitutive model and the strain localization are combined to derive a closed set of equations governing the mechanical behavior of the material system, whose solution is discussed as well. Next, the influence of the phase widths is studied and a dimensionless quantity for the spatial distribution of the plastic slip and back stress is derived, after which this work is concluded.

Notation. In this work, unless mentioned otherwise, tensors of zeroth, first and second order are denoted by italic letters, for example, a, lowercase boldface letters, for example, $\boldsymbol{a}$, and uppercase boldface letters, for example, $\boldsymbol{A}$, respectively. Tensors of higher orders are denoted as blackboard bold uppercase letters, for example, $\mathbb{A}$. The inner product is defined via $\boldsymbol{a} \cdot \boldsymbol{b} = |\boldsymbol{a}||\boldsymbol{b}| \cos(\angle(\boldsymbol{a}, \boldsymbol{b}))$ and the outer product by $(\boldsymbol{a} \otimes \boldsymbol{b})\boldsymbol{c} = \boldsymbol{a}(\boldsymbol{b} \cdot \boldsymbol{c})$. Additionally, the symmetrized outer product is denoted as $\boldsymbol{a} \otimes^{\mathrm{s}} \boldsymbol{b} = \mathrm{sym}(\boldsymbol{a} \otimes \boldsymbol{b})$. The linear mapping between tensors of order two is denoted by $\boldsymbol{A} = \mathbb{B}[\boldsymbol{C}]$. The transpose of second-order tensors is denoted by $\bullet^T$. The inverse of a fourth-order tensor $\mathbb{A}$ is defined by $\mathbb{A}\mathbb{A}^{-1} = \mathbb{I}$, with $\mathbb{I}$ being the identity on the (sub-)space at hand. The jump of a tensorial field at a singular surface is $[\![\bullet]\!] = \bullet^+ - \bullet^-$, with $\bullet^+$ and $\bullet^-$ being the right-sided and left-sided limit of $\bullet$ respectively. The volume average of a tensor field is denoted as $\langle \bullet \rangle := \int_V \bullet \mathrm{d}V/V$. If the averaging operation is only done on a subvolume $V^\xi \subseteq V$, the subvolume is explicitly stated as $\langle \bullet \rangle^\xi := \int_{V^\xi} \bullet \mathrm{d}V/V^\xi$. The partial derivatives of tensor fields with unidirectional spatial dependency with respect to the corresponding coordinate are denoted by $\boldsymbol{A}(y)' := \partial \boldsymbol{A}(y)/\partial y$. Summation over tensor indices is implicit, however a direct tensor notation is preferred throughout this text. The summation over other indices is explicitly stated. Vectors and Matrices are single and double underlined respectively. Matrix inverses and transposes are denoted with $\bullet^{-1}$ and $\bullet^T$.

2 | THEORY

2.1 | Kinematics

The geometric linear theory is based on the infinitesimal strain tensor $\boldsymbol{\varepsilon} = \mathrm{sym}(\boldsymbol{H})$, that is, the symmetrization of the displacement gradient $\boldsymbol{H} = \mathrm{grad}\,(\boldsymbol{u})$. The strain tensor is additively decomposed into an elastic part and a plastic part, that is, $\boldsymbol{\varepsilon} = \boldsymbol{\varepsilon}_\mathrm{e} + \boldsymbol{\varepsilon}_\mathrm{p}$. The elastic part $\boldsymbol{\varepsilon}_\mathrm{e}$ contains the lattice deformation due to elastic stretching, whereas the plastic part $\boldsymbol{\varepsilon}_\mathrm{p}$ captures the lattice deformation due to glissile dislocation movement. In the context of classical crystal plasticity, the plastic strain tensor reads

$$\boldsymbol{\varepsilon}_{\mathrm{p}} = \sum_{\alpha=1}^{N} \gamma_\alpha \boldsymbol{M}_\alpha, \tag{1}$$

$$\gamma_\alpha = \int \dot{\gamma}_\alpha \mathrm{d}t. \tag{2}$$

Here, γ_α are the *unsigned* plastic slips, in the following called slip parameters. These parameters are non-negative by definition, as they are obtained by integrating the corresponding nonnegative slip rates $\dot{\gamma}_\alpha \in \mathbb{R}_{\geq 0}$ resulting to monotonic functions $\gamma_\alpha \in \mathbb{R}_{\geq 0}$. The direction along which the slip occurs is given by the *signed* Schmid tensors $\boldsymbol{M}_\alpha = \boldsymbol{d}_\alpha \otimes^{\mathrm{s}} \boldsymbol{n}_\alpha$, which characterize the slip systems by their slip plane normals $\boldsymbol{n}_\alpha$ and the slip directions $\boldsymbol{d}_\alpha$. Note, that two Schmid tensors are assigned to each physical slip system to account for movement in two opposite directions, so that the number of signed slip systems N doubles the amount of physical slip systems [3].

2.2 | Field, constitutive and constraint equations

We are interested in quasi-static processes with vanishing force and moment densities, for which the balances of linear and angular momentum simplify to

$$\mathrm{div}\,(\boldsymbol{\sigma}) = \mathbf{0}, \tag{3}$$

$$\boldsymbol{\sigma} = \boldsymbol{\sigma}^T. \tag{4}$$

The Cauchy stress tensor $\boldsymbol{\sigma}$ and the infinitesimal strain tensor $\boldsymbol{\varepsilon}$ are connected by the invertible, affine maps

$$\boldsymbol{\sigma} = \mathbb{C}[\boldsymbol{\varepsilon} - \boldsymbol{\varepsilon}_{\mathrm{p}}], \tag{5}$$

$$\boldsymbol{\varepsilon} = \mathbb{S}[\boldsymbol{\sigma}] + \boldsymbol{\varepsilon}_{\mathrm{p}}, \tag{6}$$

where $\mathbb{C}$ and $\mathbb{S}$ are the stiffness and compliance tensor, respectively, with $\mathbb{C}\mathbb{S} = \mathbb{I}^{\mathrm{S}}$, where $\mathbb{I}^{\mathrm{S}}$ is the fourth-order identity tensor on the subspace of symmetric second-order tensors.

The evolution of the plastic strain tensor can be described in two different ways. First, the rate-dependent approach models a visco-plastic evolution by describing the evolution law for the plastic slip parameters. Alternatively, the rate-independent approach introduces scalar yield functions φ_α and critical shear stresses $\tau_{\mathrm{C},\alpha}$ for all N slip systems

$$\varphi_\alpha := \boldsymbol{M}_\alpha \cdot \boldsymbol{\sigma} - \tau_{\mathrm{C},\alpha}, \tag{7}$$

which form a system of equations to be solved incrementally under consideration of the Karush–Kuhn–Tucker (KKT) conditions, cf. [17]

$$\varphi_\alpha \leq 0, \qquad \dot{\gamma}_\alpha \geq 0, \qquad \varphi_\alpha \dot{\gamma}_\alpha = 0. \tag{8}$$

A systematic approach to extend existing constitutive theories by gradient effects is proposed by [6]. Using the principle of virtual power, the field equations, that is, the standard balance of linear momentum, the micromorphic balance and their respective boundary conditions are derived.

This scheme is applied to crystal plasticity and the plastic slips are chosen as the micromorphic variables to carry the gradient effects. The scalar-valued micro stresses π_α and vector-valued micro stresses $\boldsymbol{\xi}_\alpha$ are then introduced as the work conjugate quantities for the plastic slip rates $\dot{\gamma}_\alpha$ and their planar gradient $\nabla_{\mathrm{p}}\dot{\gamma}_\alpha$ which are coupled via the microforce balance [11]

$$\boldsymbol{M}_\alpha \cdot \boldsymbol{\sigma} + \mathrm{div}(\boldsymbol{\xi}_\alpha) - \pi_\alpha = 0. \tag{9}$$

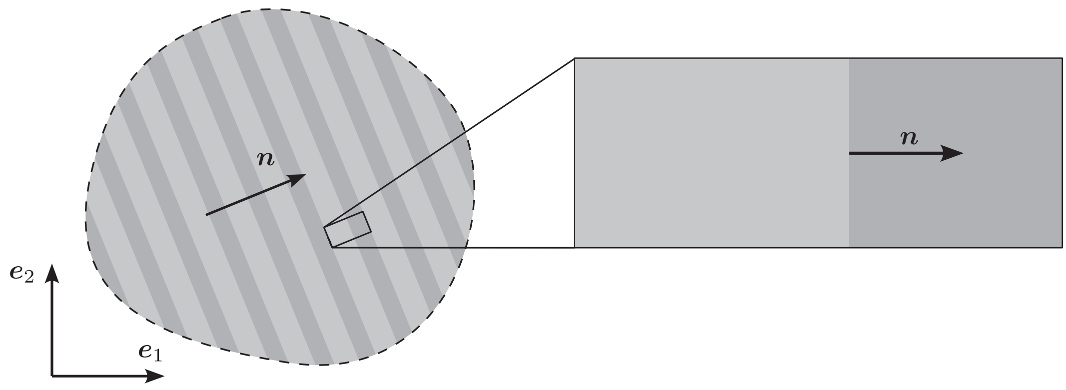

FIGURE 1 Periodic two-dimensional two-phase laminate with finite corresponding unit cell.

Note, that the subscript letter in ∇_{p} refers to the planar part of the slip gradient. This is not to be confused with the letters meaning in $\boldsymbol{\varepsilon}_{\mathrm{p}}$, where it refers to the plastic part of the infinitesimal strain tensor. For the constitutive relations of the vector-valued micro stresses we assume

$$\boldsymbol{\xi}_\alpha = K_{\mathrm{g},\alpha} \nabla_{\mathrm{p}}(\gamma_\alpha - \gamma_{\overleftarrow{\alpha}}), \tag{10}$$

$$\nabla_{\mathrm{p}}\gamma_\alpha = (\boldsymbol{I} - \boldsymbol{n}_\alpha \otimes \boldsymbol{n}_\alpha)\nabla\gamma_\alpha. \tag{11}$$

Due to the usage of unsigned plastic slips, the gradient stress involves the difference of the plastic slips corresponding to different slip directions. For any given signed slip system α, we denote the opposite slip system with $\overleftarrow{\alpha}$. Although the gradient fields, that is, the plastic slips, are scalar quantities, we can account for directional information by distinguishing their slip directions. These opposite directed slips can interact, limiting the influence of the gradient variable during cyclic loading. This circumvents the conceptual difficulties arising in theories with one scalar plastic field which is discussed by [32]. Under monotonic loading the influence of the gradient field is still unlimited, in the sense that the back stress does not saturate. This can be circumvented by using, for example, a formulation based on saturating variables [1].

Analogously to above, modified yield conditions φ_α are formulated for all slip systems

$$\varphi_\alpha := \boldsymbol{M}_\alpha \cdot \boldsymbol{\sigma} + \mathrm{div}(\boldsymbol{\xi}_\alpha) - \tau_{\mathrm{C},\alpha}, \tag{12}$$

which must comply with the KKT conditions. For a detailed derivation and discussion of the thermodynamic consistency, see, for example, [5].

2.3 | Laminate mechanics

In this article, a laminate is a d-dimensional structure denoted by $\mathcal{B}$, whose properties are translationally invariant in d-1 orthogonal directions as depicted in Figure 1. The remaining direction is called the lamination direction and denoted by $\boldsymbol{n}$. This definition includes materials with continuous properties but also the classical multiphase composites consisting of distinct phases. Points at which the property fields are differentiable are called regular points in contrast to singular points, where the fields are not differentiable. Due to the unidirectional spatial dependence, the singular points form d-1 dimensional planes which separate the regular domains between them. In the following, the planes of singular points are called *interfaces* and denoted by $\mathcal{S}$ and the regular volumes are *layers* or *phases*.

In general, this translational invariance implies that a tensor field of arbitrary order $\mathbb{T}$ can only spatially vary in direction of $\boldsymbol{n}$

$$\mathbb{T}(\boldsymbol{x}) = \mathbb{T}(\boldsymbol{x} \cdot \boldsymbol{n}) := \mathbb{T}(x). \tag{13}$$

This implies the following form for the common differential operators

$$\mathrm{grad}\,(\mathbb{T}(x)) = \mathbb{T}'(x) \otimes \boldsymbol{n}, \tag{14}$$

$$\mathrm{div}\,(\mathbb{T}(x)) = \mathbb{T}'(x)\boldsymbol{n}, \tag{15}$$

$$\mathrm{curl}\,(\boldsymbol{T}(x)) = \epsilon_{ilk} T'_{jk} n_l \boldsymbol{e}_i \otimes \boldsymbol{e}_j. \tag{16}$$

These expressions allow the formulation of two constraints for the stress and strain field within the laminate.

Equilibrium. Evaluating the balance of linear momentum in the layers implies a constant traction vector $\boldsymbol{t} = \boldsymbol{\sigma n}$ on planes parallel to the lamination direction. On the interfaces, the balance of linear momentum additionally implies $[\![\boldsymbol{\sigma n}]\!] = \boldsymbol{0}$. Combining both domains then gives the *equilibrium condition*, stating that $\boldsymbol{\sigma n}$ is constant at all points inside the whole laminate

$$\left.\begin{array}{r} \mathrm{div}\,(\boldsymbol{\sigma}) = \boldsymbol{0} \implies \boldsymbol{\sigma n} = \text{const. } \forall \boldsymbol{x} \in \mathcal{B} \setminus \mathcal{S} \\ [\![\boldsymbol{\sigma n}]\!] = \boldsymbol{0}\ \forall \boldsymbol{x} \in \mathcal{S} \end{array}\right\} \boldsymbol{\sigma n} = \text{const. } \forall \boldsymbol{x} \in \mathcal{B}. \tag{17}$$

Compatibility. A similar constraint can be derived for the displacement gradient using the integrability condition $\mathrm{curl}\,(\boldsymbol{H}) = \boldsymbol{0}$, which ensures that the displacement gradient $\boldsymbol{H}$ is integrable to a unique displacement field. The evaluation states that $\boldsymbol{Hm}$ is layer-wise constant, where $\boldsymbol{m}$ is an arbitrary vector orthogonal to $\boldsymbol{n}$. At the interface itself, we make use of its assumed coherency, such that the displacement field is continuous across it. This implies that $[\![\boldsymbol{H}]\!] = \boldsymbol{a} \otimes \boldsymbol{n}$, that is, the displacement gradient is rank 1 connected (cf. chapter 2 in [29]). Again, the constraint of the layers and the interfaces can be combined, yielding the *compatibility condition*

$$\left.\begin{array}{r} \mathrm{curl}\,(\boldsymbol{H}) = \boldsymbol{0} \implies \boldsymbol{Hm} = \text{const.} \quad \forall \boldsymbol{x} \in \mathcal{B} \setminus \mathcal{S} \\ [\![\boldsymbol{H}]\!] = \boldsymbol{a} \otimes \boldsymbol{n} \implies [\![\boldsymbol{Hm}]\!] = \boldsymbol{0} \quad \forall \boldsymbol{x} \in \mathcal{S} \end{array}\right\} \boldsymbol{Hm} = \text{const. } \forall \boldsymbol{x} \in \mathcal{B}. \tag{18}$$

These two conditions must hold for all laminates, regardless of whether the material properties vary continuously or discontinuously in direction of $\boldsymbol{n}$ and regardless of the specific constitutive model for the stress.

Since both the stress and the strain measure are symmetric, it is useful to reformulate Equations (17) and (18) for symmetric tensors, by introducing the subspaces of *exterior* and *interior* symmetric second order tensors, denoted by $\mathcal{V}_\perp$ and $\mathcal{V}_\parallel$, respectively

$$\mathcal{V}_\perp = \{\boldsymbol{A}_\perp = \boldsymbol{b} \otimes^{\mathrm{s}} \boldsymbol{n} | \boldsymbol{b} \in \mathbb{R}^d\}, \tag{19}$$

$$\mathcal{V}_\parallel = \{\boldsymbol{A}_\parallel | \boldsymbol{A}_\parallel \boldsymbol{n} = \boldsymbol{0}\}. \tag{20}$$

The projectors which project onto the subspaces are also known as *interfacial operators* [13] and decompose any symmetric second-order tensor into their exterior, that is, out-of-plane, and interior, that is, in-plane, part by $\boldsymbol{A} = \mathbb{P}_\perp[\boldsymbol{A}] + \mathbb{P}_\parallel[\boldsymbol{A}]$.

The projectors $\mathbb{P}_\perp$ and $\mathbb{P}_\parallel$ have the following explicit form (cf. Chapter 9 in [18])

$$\mathbb{P}_\perp := \frac{1}{2}\left(\boldsymbol{n} \otimes \boldsymbol{I} \otimes \boldsymbol{n} + (\boldsymbol{n} \otimes \boldsymbol{I} \otimes \boldsymbol{n})^{T_R} + (\boldsymbol{n} \otimes \boldsymbol{I} \otimes \boldsymbol{n})^{T_L} + (\boldsymbol{n} \otimes \boldsymbol{I} \otimes \boldsymbol{n})^{T_M}\right) - \boldsymbol{n} \otimes \boldsymbol{n} \otimes \boldsymbol{n} \otimes \boldsymbol{n}, \tag{21}$$

$$\mathbb{P}_\parallel := \mathbb{I}^{\mathrm{S}} - \mathbb{P}_\perp. \tag{22}$$

Here, $\bullet^{T_R}$, $\bullet^{T_L}$, and $\bullet^{T_M}$ denote the minor right, minor left, and major transposition, that is, $A^{T_R}_{ijkl} = A_{ijlk}$, $A^{T_L}_{ijkl} = A_{jikl}$, and $A^{T_M}_{ijkl} = A_{klij}$. By construction, they possess the usual projector properties of idempotency, orthogonality and completeness

$$\mathbb{P}_\perp = \mathbb{P}_\perp \mathbb{P}_\perp, \tag{23}$$

$$\mathbb{P}_\parallel = \mathbb{P}_\parallel \mathbb{P}_\parallel, \tag{24}$$

$$\mathbb{O} = \mathbb{P}_{\perp}\mathbb{P}_{\parallel}, \tag{25}$$

$$\mathbb{I}^{\mathrm{S}} = \mathbb{P}_{\perp} + \mathbb{P}_{\parallel}. \tag{26}$$

These projectors can be used to express the equilibrium and compatibility conditions, which state that the out-of-plane part of the stress tensor and the in-plane part of the strain tensor are constant, compactly by stating that the stress and strain fluctuations lie in the orthogonal subspace

$$\mathbb{P}_{\perp}[\boldsymbol{\sigma} - \langle\boldsymbol{\sigma}\rangle] = \mathbf{0} \Longrightarrow \boldsymbol{\sigma} - \langle\boldsymbol{\sigma}\rangle \in \mathcal{V}_{\parallel}, \tag{27}$$

$$\mathbb{P}_{\parallel}[\boldsymbol{\varepsilon} - \langle\boldsymbol{\varepsilon}\rangle] = \mathbf{0} \Longrightarrow \boldsymbol{\varepsilon} - \langle\boldsymbol{\varepsilon}\rangle \in \mathcal{V}_{\perp}. \tag{28}$$

A thorough discussion of these subspaces is given by [12]. For the exemplary case $d = 3$ and $\boldsymbol{n} = \boldsymbol{e}_1$, the stress and strain tensor have the following form, where the spatial dependency of the components is explicitly stated

$$\boldsymbol{\sigma}(x) \mathrel{\widehat{=}} \begin{bmatrix} \sigma_{11} & \sigma_{12} & \sigma_{13} \\ \sigma_{12} & \sigma_{22}(x) & \sigma_{23}(x) \\ \sigma_{13} & \sigma_{23}(x) & \sigma_{33}(x) \end{bmatrix}, \qquad \boldsymbol{\varepsilon}(x) \mathrel{\widehat{=}} \begin{bmatrix} \varepsilon_{11}(x) & \varepsilon_{12}(x) & \varepsilon_{13}(x) \\ \varepsilon_{12}(x) & \varepsilon_{22} & \varepsilon_{23} \\ \varepsilon_{13}(x) & \varepsilon_{23} & \varepsilon_{33} \end{bmatrix}.$$

2.4 | Stress and strain localization

We seek the relationship between the macroscopic stress $\overline{\boldsymbol{\sigma}}$ and macroscopic strain $\overline{\boldsymbol{\varepsilon}}$. In the absence of cracks and pores, the effective quantities are the volume averaged fields

$$\overline{\boldsymbol{\sigma}} = \langle\boldsymbol{\sigma}(\boldsymbol{x})\rangle,$$

$$\overline{\boldsymbol{\varepsilon}} = \langle\boldsymbol{\varepsilon}(\boldsymbol{x})\rangle.$$

In the case of an affine constitutive relation for the stress, such as small-strain elastoplasticity or thermoelasticity, the localization can be expressed as the affine maps

$$\boldsymbol{\varepsilon}(\boldsymbol{x}) = \mathbb{A}(\boldsymbol{x})[\overline{\boldsymbol{\varepsilon}}] - \boldsymbol{a}(\boldsymbol{x}), \tag{29}$$

$$\boldsymbol{\sigma}(\boldsymbol{x}) = \mathbb{B}(\boldsymbol{x})[\overline{\boldsymbol{\sigma}}] - \boldsymbol{b}(\boldsymbol{x}), \tag{30}$$

where $\mathbb{A}$ and $\mathbb{B}$ are the strain and stress localization tensors and $\boldsymbol{a}$ and $\boldsymbol{b}$ are the strain and stress fluctuations, which vanish for the linear elastic case. In general, the tensor fields depend on the material properties and on the inelastic strain. Closed-form expressions for these tensors are generally not accessible due to the high complexity of the microstructure. Note that the complete knowledge of these tensors corresponds to the complete solution of the problem.

An exception to this is the periodic laminate for which the exact relations were derived by [12]. In the original derivation by [12], the presence of interfaces is required to introduce the subspaces $\mathcal{V}_{\perp}$ and $\mathcal{V}_{\parallel}$. This is not necessary, since the subspaces can be motivated in their absence using only the translational invariance of the structure normal to the lamination direction as discussed above. Once the subspaces for the stress and strain fluctuations are motivated, the localizations can be derived to be ([12] or Appendix A)

$$\boldsymbol{\varepsilon} = (\mathbb{S}\mathbb{Z} + \mathbb{K}\langle\mathbb{K}\rangle^{\dagger}\langle\mathbb{K}\mathbb{C}\rangle)[\overline{\boldsymbol{\varepsilon}}] + \mathbb{K}\mathbb{C}[\boldsymbol{\varepsilon}_{\mathrm{p}}] - \mathbb{K}\langle\mathbb{K}\rangle^{\dagger}\langle\mathbb{K}\mathbb{C}[\boldsymbol{\varepsilon}_{\mathrm{p}}]\rangle, \tag{31}$$

$$\boldsymbol{\sigma} = (\mathbb{C}\mathbb{K} + \mathbb{Z}\langle\mathbb{Z}\rangle^{\dagger}\langle\mathbb{Z}\mathbb{S}\rangle)[\overline{\boldsymbol{\sigma}}] - \mathbb{Z}[\boldsymbol{\varepsilon}_{\mathrm{p}}] + \mathbb{Z}\langle\mathbb{Z}\rangle^{\dagger}\langle\mathbb{Z}[\boldsymbol{\varepsilon}_{\mathrm{p}}]\rangle, \tag{32}$$

where the auxiliary tensors can be expressed with the generalized inverse $\bullet^{\dagger}$ as

$$\mathbb{K} := (\mathbb{P}_{\perp}\mathbb{C}\mathbb{P}_{\perp})^{\dagger}, \ \text{s.t.}\ \mathbb{K}(\mathbb{P}_{\perp}\mathbb{C}\mathbb{P}_{\perp}) = \mathbb{P}_{\perp}, \tag{33}$$

$$\mathbb{Z} := (\mathbb{P}_{\parallel}\mathbb{S}\mathbb{P}_{\parallel})^{\dagger}, \ \text{s.t.}\ \mathbb{Z}(\mathbb{P}_{\parallel}\mathbb{S}\mathbb{P}_{\parallel}) = \mathbb{P}_{\parallel}. \tag{34}$$

These auxiliary tensors also appear in the context of interfaces [31] and can, for example, be used to express the jumps of the strain and stress tensor at an interface between two elastic solids in terms of the one-sided limits

$$[\![\boldsymbol{\varepsilon}]\!] = -\mathbb{K}^{\pm}[\![\mathbb{C}]\!][\boldsymbol{\varepsilon}^{\mp}] \tag{35}$$

$$[\![\boldsymbol{\sigma}]\!] = -\mathbb{Z}^{\pm}[\![\mathbb{S}]\!][\boldsymbol{\sigma}^{\mp}]. \tag{36}$$

Additionally, $\mathbb{K}$ can be expressed in terms of the acoustic Tensor $L_{ik} = C_{ijkl}n_j n_l$ by $4K_{ijkl} = L^{-1}_{ik}n_j n_l + L^{-1}_{jk}n_i n_l + L^{-1}_{il}n_j n_k + L^{-1}_{jl}n_i\, n_k$.The auxiliary tensors are interconnected with the stiffness and compliance tensors by

$$\mathbb{C}\mathbb{K} + \mathbb{Z}\mathbb{S} = \mathbb{K}\mathbb{C} + \mathbb{S}\mathbb{Z} = \mathbb{I}^{\mathrm{S}}. \tag{37}$$

A thorough discussion of the auxiliary tensors is given by [13] as well as [31].

Comparing coefficients with Equations (29) and (30) yields the localizations tensors

$$\mathbb{A} = \mathbb{S}\mathbb{Z} + \mathbb{K}\langle\mathbb{K}\rangle^{\dagger}\langle\mathbb{K}\mathbb{C}\rangle, \tag{38}$$

$$\boldsymbol{a} = -\mathbb{K}\mathbb{C}[\boldsymbol{\varepsilon}_{\mathrm{p}}] + \mathbb{K}\langle\mathbb{K}\rangle^{\dagger}\langle\mathbb{K}\mathbb{C}[\boldsymbol{\varepsilon}_{\mathrm{p}}]\rangle, \tag{39}$$

$$\mathbb{B} = \mathbb{C}\mathbb{K} + \mathbb{Z}\langle\mathbb{Z}\rangle^{\dagger}\langle\mathbb{Z}\mathbb{S}\rangle, \tag{40}$$

$$\boldsymbol{b} = \mathbb{Z}[\boldsymbol{\varepsilon}_{\mathrm{p}}] - \mathbb{Z}\langle\mathbb{Z}\rangle^{\dagger}\langle\mathbb{Z}[\boldsymbol{\varepsilon}_{\mathrm{p}}]\rangle. \tag{41}$$

This result is valid for arbitrary functions of the stiffness and eigenstrain tensors in the form $\mathbb{C}(\boldsymbol{x}) = \mathbb{C}(x)$ and $\boldsymbol{\varepsilon}_{\mathrm{p}}(\boldsymbol{x}) = \boldsymbol{\varepsilon}_{\mathrm{p}}(x)$, that is, as long as their translational invariance normal to $\boldsymbol{n}$ is preserved. Inserting the strain localization into Hooke's law and making use of Equation (37) yields the local stress field

$$\begin{aligned}\boldsymbol{\sigma} &= \mathbb{C}[\boldsymbol{\varepsilon} - \boldsymbol{\varepsilon}_{\mathrm{p}}] \\ &= \mathbb{C}[\mathbb{A}[\overline{\boldsymbol{\varepsilon}}] - \boldsymbol{a} - \boldsymbol{\varepsilon}_{\mathrm{p}}] \\ &= \mathbb{C}\mathbb{A}[\overline{\boldsymbol{\varepsilon}}] - \mathbb{C}(\mathbb{I}^{\mathrm{S}} - \mathbb{K}\mathbb{C})[\boldsymbol{\varepsilon}_{\mathrm{p}}] - \mathbb{C}\mathbb{K}\langle\mathbb{K}\rangle^{\dagger}\langle\mathbb{K}\mathbb{C}[\boldsymbol{\varepsilon}_{\mathrm{p}}]\rangle \\ &= \mathbb{C}\mathbb{A}[\overline{\boldsymbol{\varepsilon}}] - \mathbb{Z}[\boldsymbol{\varepsilon}_{\mathrm{p}}] - \mathbb{C}\mathbb{K}\langle\mathbb{K}\rangle^{\dagger}\langle\mathbb{K}\mathbb{C}[\boldsymbol{\varepsilon}_{\mathrm{p}}]\rangle.\end{aligned} \tag{42}$$

We focus on material systems with M distinct phases, such that the stiffness is piecewise constant but the plastic strain is inhomogeneous. Splitting the averaging operator as follows

$$\langle\bullet\rangle = \sum_{\eta=1}^{M} c^{\eta}\langle\bullet\rangle^{\eta}, \qquad \langle\bullet\rangle^{\eta} := \frac{1}{V^{\eta}}\int_{V^{\eta}}(\bullet)\mathrm{d}V \tag{43}$$

and using the linearity of integration, the last term in Equation (42) can be rewritten as

$$\mathbb{C}\mathbb{K}\langle\mathbb{K}\rangle^{\dagger}\langle\mathbb{K}\mathbb{C}[\boldsymbol{\varepsilon}_{\mathrm{p}}]\rangle = \mathbb{C}\mathbb{K}\langle\mathbb{K}\rangle^{\dagger}\sum_{\eta=1}^{M} c^{\eta}\mathbb{K}^{\eta}\mathbb{C}^{\eta}[\langle\boldsymbol{\varepsilon}_{\mathrm{p}}\rangle^{\eta}]. \tag{44}$$

This motivates the introduction of the phase-wise constant auxiliary fourth-order tensor

$$\mathbb{Y}^{\eta} := c^{\eta}\langle\mathbb{K}\rangle^{\dagger}\mathbb{K}^{\eta}\mathbb{C}^{\eta}, \tag{45}$$

which allows to express the local stresses as

$$\boldsymbol{\sigma} = \mathbb{C}\mathbb{A}[\overline{\boldsymbol{\varepsilon}}] - \mathbb{Z}[\boldsymbol{\varepsilon}_{\mathrm{p}}] - \mathbb{C}\mathbb{K}\sum_{\eta=1}^{M}\mathbb{Y}^{\eta}[\langle\boldsymbol{\varepsilon}_{\mathrm{p}}\rangle^{\eta}]. \tag{46}$$

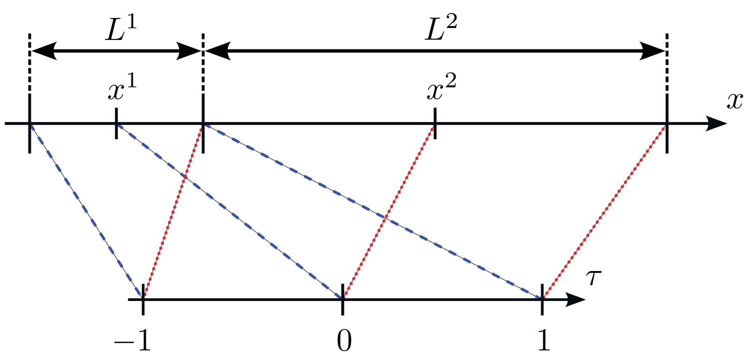

FIGURE 2 Phase-wise mapping between physical position x and the dimensionless coordinate τ. The mapping of phase 1 (dashed, blue) and that of phase 2 (dotted, red).

2.5 | Matrix formulation

In order to derive a system of equations which describes the evolution of the plastic deformation, we proceed as follows. Inserting the local stress Equation (46) and slip system based plastic strain tensor Equation (1) into the yield functions, Equation (12) reads:

$$\varphi^{\xi}_{\alpha} = \boldsymbol{M}^{\xi}_{\alpha} \cdot \mathbb{C}^{\xi}\mathbb{A}^{\xi}[\overline{\boldsymbol{\varepsilon}}] - \boldsymbol{M}^{\xi}_{\alpha} \cdot \mathbb{Z}^{\xi}\left[\sum_{\beta=1}^{N_{\xi}} \boldsymbol{M}^{\xi}_{\beta}\gamma^{\xi}_{\beta}\right]$$
$$- \boldsymbol{M}^{\xi}_{\alpha} \cdot \mathbb{C}^{\xi}\mathbb{K}^{\xi}\sum_{\eta=1}^{M}\left[\mathbb{Y}^{\eta}\left[\sum_{\beta=1}^{N_{\eta}} \boldsymbol{M}^{\eta}_{\beta}\langle\gamma^{\eta}_{\beta}\rangle^{\eta}\right]\right] + \operatorname{div}\left(K^{\xi}_{\mathrm{g},\alpha}\nabla^{\xi}_{\mathrm{p},\alpha}\left(\gamma^{\xi}_{\alpha} - \gamma^{\xi}_{\bar{\alpha}}\right)\right) - \tau^{\xi}_{\mathrm{C},\alpha}. \tag{47}$$

Here, the superscript indices $\xi, \eta \in \mathbb{N}$ are introduced to distinguish between different phases. Additionally, the subscript indices $\alpha, \beta \in \mathbb{N}$ are used to denote tensors associated with different slip systems within the phases. For instance, the stiffness tensor within phase ξ with $\xi = \{1, \dots, M\}$ is therefore denoted by $\mathbb{C}^{\xi}$. The slip system specific quantities within phase ξ require the additional index α with $\alpha = \{1, \dots, N_{\xi}\}$, where N_{ξ} is the number of slip systems within phase ξ. The Schmid tensor of the αth slip system within phase ξ is thus denoted by $\boldsymbol{M}^{\xi}_{\alpha}$ for example. Additionally, we split up the averaging operation of the plastic strain tensor into averages of the phase and slip system specific plastic slips, that is,

$$\langle\boldsymbol{\varepsilon}_{\mathrm{p}}\rangle^{\eta} = \left\langle\sum_{\alpha=1}^{N_{\alpha}} \boldsymbol{M}^{\eta}_{\alpha}\gamma^{\eta}_{\alpha}\right\rangle^{\eta} = \sum_{\alpha=1}^{N_{\alpha}} \boldsymbol{M}^{\eta}_{\alpha}\left\langle\gamma^{\eta}_{\alpha}\right\rangle^{\eta}. \tag{48}$$

We concatenate all yield functions of all slip systems from Equation (47) into the vector $\underline{\varphi} \in \mathbb{R}^{\mathcal{N}}$ with the total number of slip system $\mathcal{N} = N_1 + N_2 + \dots + N_M$, that is, $\underline{\varphi} = \{\varphi^1_1, \varphi^1_2, \dots, \varphi^M_{N_M}\}$. Analogously, the vectors $\underline{\gamma}, \underline{\gamma}''$ and $\langle\underline{\gamma}\rangle$, corresponding to the slip parameters, their second spatial derivative and their phase-wise mean are assembled. Since the function domains of $\varphi^{\xi}_{\alpha}(x)$ are different, we make use of the following phase-wise coordinate transformation from the position x to the non dimensional coordinate $\tau \in [-1, 1]$

$$x = x^{\xi} + \tau\frac{L^{\xi}}{2}, \tag{49}$$

where x^{ξ} and L^{ξ} are the coordinates of the phase center and the phase width, respectively. This maps the phase centers to $\tau = 0$ and the phase boundary to $\tau = -1$ and $\tau = 1$ as visualized in Figure 2.

The linear transformation directly implies the following relations

$$f^{\xi}(\tau) = g^{\xi}(x), \tag{50}$$

$$f^{\xi}(\tau)'' = \frac{\mathrm{d}^2 f^{\xi}(\tau)}{\mathrm{d}\tau^2} = \frac{\mathrm{d}^2 g^{\xi}(x)}{\mathrm{d}x^2}\left(\frac{\mathrm{d}x}{\mathrm{d}\tau}\right)^2 = g^{\xi}(x)''\left(\frac{L^{\xi}}{2}\right)^2, \tag{51}$$

$$\langle f^{\xi}(\tau)\rangle^{\xi} = \frac{1}{2}\int_{-1}^{1} f^{\xi}(\tau)\mathrm{d}\tau = \frac{1}{L^{\xi}}\int_{-L^{\xi}/2}^{L^{\xi}/2} g^{\xi}(x)\mathrm{d}x = \langle g^{\xi}(x)\rangle^{\xi}. \tag{52}$$

This allows the formulation of the vectors in terms of the nondimensional coordinate τ as

$$\underline{\gamma}(\tau) := \begin{bmatrix} \gamma_1^1(\tau) \\ \gamma_2^1(\tau) \\ \vdots \\ \gamma_{N_M}^M(\tau) \end{bmatrix}, \qquad \underline{\gamma}(\tau)'' := \begin{bmatrix} \gamma_1^1(\tau)'' \\ \gamma_2^1(\tau)'' \\ \vdots \\ \gamma_{N_M}^M(\tau)'' \end{bmatrix}, \qquad \langle\underline{\gamma}(\tau)\rangle := \begin{bmatrix} \langle\gamma_1^1(\tau)\rangle^1 \\ \langle\gamma_2^1(\tau)\rangle^1 \\ \vdots \\ \langle\gamma_{N_M}^M(\tau)\rangle^M \end{bmatrix}. \tag{53}$$

The yield functions can then be expressed by a vector-matrix notation

$$\underline{\varphi}(\tau) = -\underline{\underline{A}}\,\underline{\gamma}(\tau) + \underline{\underline{B}}\,\underline{\gamma}(\tau)'' - \underline{\underline{C}}\,\langle\underline{\gamma}(\tau)\rangle - \underline{c}, \tag{54}$$

where the coefficient matrices $\underline{\underline{A}}, \underline{\underline{B}}, \underline{\underline{C}} \in \mathbb{R}^{\mathcal{N}\times\mathcal{N}}$ are assembled from the corresponding prefactors and the vector $\underline{c} \in \mathbb{R}^{\mathcal{N}}$ collects the remaining terms. The structure and properties of $\underline{\underline{A}}$, $\underline{\underline{B}}$, $\underline{\underline{C}}$ and $\underline{c}$ are briefly discussed in the following with more details in Appendix C.

The matrix $\underline{\underline{A}}$ has a block diagonal structure consisting of the symmetric submatrices $\underline{\underline{A}}^{\xi} \in \mathbb{R}^{N_{\xi}\times N_{\xi}}$ which couple the yield conditions within the same phase. The matrix $\underline{\underline{A}}$ and the components of its submatrices $\underline{\underline{A}}^{\xi}$ are given by

$$\underline{\underline{A}} = \text{block-diag}(\underline{\underline{A}}^1, \underline{\underline{A}}^2, \dots, \underline{\underline{A}}^M), \qquad A^{\xi}_{\alpha\beta} = \boldsymbol{M}^{\xi}_{\alpha}\cdot\mathbb{Z}^{\xi}[\boldsymbol{M}^{\xi}_{\beta}]. \tag{55}$$

The matrix $\underline{\underline{B}}$ models the contribution of the vector-valued stress towards the yield functions and therefore captures the gradient effects. The structure of $\underline{\underline{B}}$ is again block-diagonal with submatrices $\underline{\underline{B}}^{\xi} \in \mathbb{R}^{N_{\xi}\times N_{\xi}}$ which are block-diagonal themselves due to neglected interaction between the dislocation pileups of different slip systems. Note, that the slip gradient within the same slip system can interact, which couples the slip system α with its opposite $\overleftarrow{\alpha}$, such that the block-matrices within $\underline{\underline{B}}^{\xi}$ are $\in \mathbb{R}^{2\times 2}$.

The matrix $\underline{\underline{B}}$ and the components of its submatrices $\underline{\underline{B}}^{\xi}$ are given by

$$\underline{\underline{B}} = \text{block-diag}(\underline{\underline{B}}^1, \underline{\underline{B}}^2, \dots, \underline{\underline{B}}^M), \qquad B^{\xi}_{\alpha\beta} = K^{\xi}_{\mathrm{g},\alpha}\left(1 - (\boldsymbol{n}^{\xi}_{\alpha}\cdot\boldsymbol{n})^2\right)\left(\frac{2}{L^{\xi}}\right)^2 \varrho_{\alpha\beta}, \tag{56}$$

where $\varrho_{\alpha\beta}$ accounts for the coupling between different slip direction of the same, which is defined as

$$\varrho_{\alpha\beta} = \begin{cases} 1, & \text{for } \beta = \alpha \\ -1, & \text{for } \beta = \overleftarrow{\alpha} \\ 0, & \text{else.} \end{cases} \tag{57}$$

In order to arrive at the compact form from Equation (56), we make use of the differential operator for unidirectional fields (Equations (14) and (15)) to find

$$\begin{aligned} \operatorname{div}\left(K^{\xi}_{\mathrm{g},\alpha}\nabla^{\xi}_{\mathrm{p},\alpha}\gamma^{\xi}_{\alpha}\right) &= K^{\xi}_{\mathrm{g},\alpha}\operatorname{div}\left((\boldsymbol{I} - \boldsymbol{n}^{\xi}_{\alpha}\otimes\boldsymbol{n}^{\xi}_{\alpha})\nabla\gamma^{\xi}_{\alpha}\right) \\ &= K^{\xi}_{\mathrm{g},\alpha}\operatorname{div}\left((\boldsymbol{I} - \boldsymbol{n}^{\xi}_{\alpha}\otimes\boldsymbol{n}^{\xi}_{\alpha})\gamma^{\xi\,\prime}_{\alpha}\boldsymbol{n}\right) \\ &= K^{\xi}_{\mathrm{g},\alpha}\left((\boldsymbol{I} - \boldsymbol{n}^{\xi}_{\alpha}\otimes\boldsymbol{n}^{\xi}_{\alpha})\gamma^{\xi\,\prime\prime}_{\alpha}\boldsymbol{n}\right)\cdot\boldsymbol{n} \\ &= K^{\xi}_{\mathrm{g},\alpha}\left(1 - (\boldsymbol{n}^{\xi}_{\alpha}\cdot\boldsymbol{n})^2\right)\gamma^{\xi\,\prime\prime}_{\alpha}. \end{aligned} \tag{58}$$

From Equation (58), we conclude directly that in slip systems with slip directions parallel to the interfaces, the back stress vanishes. This is a direct consequence of the chosen gradient energy in combination with the translational invariance of the plastic slip fields, which prohibits slip gradients perpendicular to the lamination direction. This result is also intuitive as the glide length increases infinitely in those slip systems.

In contrast to $\underline{\underline{A}}$ and $\underline{\underline{B}}$, the matrix $\underline{\underline{C}}$ has a dense block-structure consisting of submatrices $\underline{\underline{C}}^{\xi\eta} \in \mathbb{R}^{N_\xi \times N_\eta}$ which, in general, are dense themselves. $\underline{\underline{C}}$ therefore introduces a coupling between the yield conditions of the different phases. The diagonal submatrices $\underline{\underline{C}}^{\xi\xi}$ are symmetric and for the off-diagonal submatrices, the relation $c^\xi \underline{\underline{C}}^{\xi\eta} = c^\eta (\underline{\underline{C}}^{\eta\xi})^T$ holds, such that $\underline{\underline{C}}$ is only symmetric if all lamellas are of equal width. The matrix $\underline{\underline{C}}$ and the components of its submatrices $\underline{\underline{C}}^{\xi\eta}$ are given by

$$\underline{\underline{C}} = \begin{bmatrix} \underline{\underline{C}}^{11} & \underline{\underline{C}}^{12} & \cdots & \underline{\underline{C}}^{1M} \\ \underline{\underline{C}}^{21} & \underline{\underline{C}}^{22} & \cdots & \underline{\underline{C}}^{2M} \\ \vdots & \vdots & \ddots & \vdots \\ \underline{\underline{C}}^{M1} & \underline{\underline{C}}^{M2} & \cdots & \underline{\underline{C}}^{MM} \end{bmatrix}, C^{\xi\eta}_{\alpha\beta} = \boldsymbol{M}^\xi_\alpha \cdot \mathbb{C}^\xi \mathbb{K}^\xi \mathbb{Y}^\eta [\boldsymbol{M}^\eta_\beta] = c^\eta \boldsymbol{M}^\xi_\alpha \cdot \mathbb{C}^\xi \mathbb{K}^\xi \langle \mathbb{K} \rangle^\dagger \mathbb{K}^\eta \mathbb{C}^\eta [\boldsymbol{M}^\eta_\beta]. \tag{59}$$

Lastly, the vector $\underline{c}$ is assembled from the subvectors $\underline{c}^\xi \in \mathbb{R}^{N_\xi}$. In contrast to the matrices, the vector is not constant as it includes the contribution of the effective strain

$$\underline{c} = \begin{bmatrix} \underline{c}^1 \\ \underline{c}^2 \\ \vdots \\ \underline{c}^M \end{bmatrix}, \qquad c^\xi_\alpha = \tau^\xi_{\mathrm{C},\alpha} - \boldsymbol{M}^\xi_\alpha \cdot \mathbb{C}^\xi \mathbb{A}^\xi [\overline{\boldsymbol{\varepsilon}}]. \tag{60}$$

Note that the coefficient matrices $\underline{\underline{A}}$ and $\underline{\underline{C}}$ constant due to the restriction to phase-wise constant stiffness and Schmid tensors $\mathbb{C}^\xi$ and $\boldsymbol{M}^\xi_\alpha$. If we additionally assume phase-wise constant $K^\xi_{\mathrm{g},\alpha}$, $\underline{\underline{B}}$ is constant as well. These properties are required as the following solution procedure exploits the linearity of Equation (54) and the constancy of the coefficient matrices $\underline{\underline{A}}$, $\underline{\underline{B}}$ and $\underline{\underline{C}}$. For the same reason the functional dependency of $\underline{c}$ on $\underline{\gamma}$ is limited to be affine, such that the hardening mechanisms are limited to linear ones. The extension to include hardening is straight forward and described in Appendix B.

2.6 | Solution procedure

In this section, a constitutive integration algorithm for the spatially inhomogeneous plastic slips is proposed. To this end, we formulate the yield conditions for all slip systems in all phases incrementally and set them to zero, such that

$$\underline{\varphi}(\underline{\gamma}^{\mathrm{n}} + \Delta\underline{\gamma}) \stackrel{!}{=} \underline{0} \iff -\underline{\underline{A}}\,\Delta\underline{\gamma} + \underline{\underline{B}}\,\Delta\underline{\gamma}'' = \underline{\underline{C}}\,\langle \Delta\underline{\gamma} \rangle + \underline{\underline{A}}\,\underline{\gamma}^{\mathrm{n}} - \underline{\underline{B}}\,\underline{\gamma}^{\mathrm{n}\prime\prime} + \underline{\underline{C}}\,\langle \underline{\gamma}^{\mathrm{n}} \rangle + \underline{c}. \tag{61}$$

Here, the superscript $(\bullet)^{\mathrm{n}}$ is used to denote functional quantities from the previously converged step and $\Delta(\bullet)$ denotes the functional increment. The slip parameters must fulfill the discrete KKT conditions given by

$$\underline{\varphi} \odot \Delta\underline{\gamma} = \underline{0}, \quad \underline{\varphi} \leq 0, \quad \Delta\underline{\gamma} \geq 0, \tag{62}$$

where $\odot$ is the element-wise product and the inequalities state that the vectors $\underline{\varphi}$ and $\Delta\underline{\gamma}$ are element-wise nonpositive and nonnegative, respectively. The solution of Equation (61) under consideration of Equation (62) requires special attention for two reasons.

Firstly, analogously to the classical, that is, nongradient, formulation of rate-independent crystal plasticity, the set of active slip systems is not known in advance, such that an active set search is required to determine a suitable set of active slip systems iteratively. In order to derive at a discrete system of equations, we assume that the slip system activity, that is, the signs of the yield functions and slip increments, is phase-wise homogeneous. This allows the computation of the plastic slip by only considering one set of yield functions in each phase. For the active set search, we make use of the algorithm proposed by [27] to find an active set based on the values of the yield function and slip increment evaluated at the phase center. Secondly, Equation (61) is classified as a system of coupled second-order *Fredholm integro-differential equations* (FIDE) for the slip parameter increments, since the increments itself, their second spatial derivative as well as their spatial mean as an integral quantity, appear. Its solution are nonconstant functions which are required to fully describe the laminates state, and will be discussed in the following.

The set of currently active slip systems uniquely defines the matrix $\underline{\underline{L}} : \underline{\varphi} \mapsto \underline{\tilde{\varphi}}$ which extracts the yield functions of the currently active slip system $\underline{\tilde{\varphi}}$ from the full yield function vector $\underline{\varphi}$. Similarly, the inverse mapping is given by $\underline{\underline{L}}^T : \Delta\underline{\tilde{\gamma}} \mapsto \Delta\underline{\gamma}$. This maps the solution increments $\Delta\underline{\tilde{\gamma}}$ from the active set back to the full vector $\Delta\underline{\gamma}$. Inserting the relations

$$\underline{\tilde{\varphi}} = \underline{\underline{L}}\ \underline{\varphi}, \tag{63}$$

$$\Delta\underline{\gamma} = \underline{\underline{L}}^T\ \Delta\underline{\tilde{\gamma}}, \tag{64}$$

$$\Delta\underline{\gamma}'' = \underline{\underline{L}}^T\ \Delta\underline{\tilde{\gamma}}'', \tag{65}$$

$$\langle\Delta\underline{\gamma}\rangle = \underline{\underline{L}}^T\ \langle\Delta\underline{\tilde{\gamma}}\rangle, \tag{66}$$

into Equation (61) results in the reduced FIDE system for the currently active set

$$-\underbrace{\underline{\underline{L}}\ \underline{\underline{A}}\ \underline{\underline{L}}^T}_{\underline{\underline{\tilde{A}}}}\Delta\underline{\tilde{\gamma}} + \underbrace{\underline{\underline{L}}\ \underline{\underline{B}}\ \underline{\underline{L}}^T}_{\underline{\underline{\tilde{B}}}}\Delta\underline{\tilde{\gamma}}'' = \underbrace{\underline{\underline{L}}\ \underline{\underline{C}}\ \underline{\underline{L}}^T}_{\underline{\underline{\tilde{C}}}}\langle\Delta\underline{\tilde{\gamma}}\rangle + \underline{\underline{L}}\ \underline{\underline{A}}\ \underline{\gamma}^{\mathrm{n}} - \underline{\underline{L}}\ \underline{\underline{B}}\ \underline{\gamma}^{\mathrm{n}\prime\prime} + \underline{\underline{L}}\ \underline{\underline{C}}\ \langle\underline{\gamma}^{\mathrm{n}}\rangle + \underline{\underline{L}}\ \underline{c}. \tag{67}$$

As a consequence of the properties of $\underline{\underline{\tilde{A}}}$ and $\underline{\underline{\tilde{B}}}$ (cf. Appendix C), the solution of Equation (67) can be stated explicitly as a hyperbolic series, which will be motivated later

$$\Delta\underline{\gamma}(\tau) = \Delta\underline{a} + \sum_{i=1}^{\infty}\Delta\underline{b}_i \cosh(\Omega_i\tau) + \Delta\underline{d}_i \sinh(\Omega_i\tau) = \underline{\underline{L}}^T\Delta\underline{\tilde{\gamma}}. \tag{68}$$

By recursion, it is clear that the solution of the previous step can be expressed in the same way, as it is a sum of increments with the shape of Equation (68), such that

$$\underline{\gamma}^{\mathrm{n}}(\tau) = \underline{a}^{\mathrm{n}} + \sum_{i=1}^{\infty}\underline{b}_i^{\mathrm{n}} \cosh(\Omega_i\tau) + \underline{d}_i^{\mathrm{n}} \sinh(\Omega_i\tau). \tag{69}$$

Here $\Delta\underline{a}, \Delta\underline{b}_i, \Delta\underline{d}_i, \underline{a}^{\mathrm{n}}, \underline{b}_i^{\mathrm{n}}, \underline{d}_i^{\mathrm{n}} \in \mathbb{R}^{\mathcal{N}}$ are coefficient vectors and $\Omega_i \in \mathbb{R}$ the frequencies of the hyperbolic functions. We want to determine $\Delta\underline{a}, \Delta\underline{b}_i, \Delta\underline{d}_i$ and Ω_i by solving Equation (67). This is done using the direct computation method, which transforms integro-differential equations into a system of ordinary differential equations and algebraic equations [19]. The generalization to systems of Fredholm integro-differential equations is, at least for this application, straight-forward.

For this, the incremental solution is additively decomposed into three parts which all solve Equation (67) for different right-hand sides. This is possible due to the linearity of the equation. The Fredholm integro-differential equation can thus be rewritten to the equivalent system

$$\Delta\underline{\tilde{\gamma}}_1 + \Delta\underline{\tilde{\gamma}}_2 + \Delta\underline{\tilde{\gamma}}_3 = \Delta\underline{\tilde{\gamma}}, \tag{70}$$

$$-\underline{\underline{\tilde{A}}}\ \Delta\underline{\tilde{\gamma}}_1 + \underline{\underline{\tilde{B}}}\ \Delta\underline{\tilde{\gamma}}_1'' = \underline{0}, \tag{71}$$

$$-\underline{\underline{\tilde{A}}}\ \Delta\underline{\tilde{\gamma}}_2 + \underline{\underline{\tilde{B}}}\ \Delta\underline{\tilde{\gamma}}_2'' = \underline{\underline{L}}\ \underline{\underline{A}}\ (\underline{\gamma}^{\mathrm{n}} - \underline{a}^{\mathrm{n}}) - \underline{\underline{L}}\ \underline{\underline{B}}\ \underline{\gamma}^{\mathrm{n}\prime\prime}, \tag{72}$$

$$-\underline{\underline{\tilde{A}}}\ \Delta\underline{\tilde{\gamma}}_3 + \underline{\underline{\tilde{B}}}\ \Delta\underline{\tilde{\gamma}}_3'' = \underline{\underline{\tilde{C}}}\ \langle\Delta\underline{\tilde{\gamma}}_1 + \Delta\underline{\tilde{\gamma}}_2 + \Delta\underline{\tilde{\gamma}}_3\rangle + \underline{\underline{L}}\ \underline{\underline{A}}\ \underline{a}^{\mathrm{n}} + \underline{\underline{L}}\ \underline{\underline{C}}\ \langle\underline{\gamma}^{\mathrm{n}}\rangle + \underline{\underline{L}}\ \underline{c}. \tag{73}$$

The function $\Delta\underline{\tilde{\gamma}}_1$ is the *homogeneous solution* of the corresponding ODE and the functions $\Delta\underline{\tilde{\gamma}}_2$ and $\Delta\underline{\tilde{\gamma}}_3$ are the *particular solutions* for the nonconstant and the constant right-hand side, respectively. The split of a function into a constant and nonconstant part is not unique. Here we make the obvious choice, which results from the general solution, see Equation (68). Note that the emerging system is only explicitly coupled, such that $\Delta\underline{\tilde{\gamma}}_1$, $\Delta\underline{\tilde{\gamma}}_2$ and $\Delta\underline{\tilde{\gamma}}_3$ can be computed consecutively.

Additionally, the linearity of Equation (68) allows for closed-form expressions of the functions $\Delta\underline{\tilde{\gamma}}_1$, $\Delta\underline{\tilde{\gamma}}_2$ and $\Delta\underline{\tilde{\gamma}}_3$, which is outlined in the following. The function $\Delta\underline{\tilde{\gamma}}_1$ is the homogeneous solution from the ODE of the active set

$$-\underline{\underline{\tilde{A}}}\ \Delta\underline{\tilde{\gamma}}_1 + \underline{\underline{\tilde{B}}}\ \Delta\underline{\tilde{\gamma}}_1'' = \underline{0}. \tag{74}$$

Choosing the classical exponential ansatz for linear systems leads to the generalized eigenvalue problem

$$-\underline{\underline{\tilde{A}}}\ \underline{\underline{\Phi}} + \underline{\underline{\tilde{B}}}\ \underline{\underline{\Phi}}\ (\underline{\underline{\Lambda}})^2 = \underline{\underline{0}}. \tag{75}$$

Here, the matrix $\underline{\underline{\Phi}}$ contains the generalized eigenvectors and the diagonal matrix $(\underline{\underline{\Lambda}})^2$ contains the generalized eigenvalues of the pair $(\underline{\underline{\tilde{A}}}, \underline{\underline{\tilde{B}}})$. Due to the block structure of $\underline{\underline{\tilde{A}}}$ and $\underline{\underline{\tilde{B}}}$, the eigenvalue problem is decoupled for all phases, such that $\underline{\underline{\Phi}}$ and $(\underline{\underline{\Lambda}})^2$ are block-diagonal as well

$$\underline{\underline{\Phi}} := \operatorname{diag}(\underline{\underline{\Phi}}^1, \underline{\underline{\Phi}}^2, \dots, \underline{\underline{\Phi}}^M), \qquad \underline{\underline{\Phi}}^\xi = [\underline{\phi}_1^\xi, \underline{\phi}_2^\xi, \dots\ ], \tag{76}$$

$$(\underline{\underline{\Lambda}})^2 := \operatorname{diag}\Big((\underline{\underline{\Lambda}}^1)^2, (\underline{\underline{\Lambda}}^2)^2, \dots, (\underline{\underline{\Lambda}}^M)^2\Big), \qquad (\underline{\underline{\Lambda}}^\xi)^2 = \operatorname{diag}\Big((\lambda_1^\xi)^2, (\lambda_2^\xi)^2, \dots\ \Big), \tag{77}$$

with $\underline{\underline{\Phi}}^\xi$ and $(\underline{\underline{\Lambda}}^\xi)^2$ being the generalized eigenvectors and eigenvalues of $(\underline{\underline{\tilde{A}}}^\xi, \underline{\underline{\tilde{B}}}^\xi)$. Since $\underline{\underline{\tilde{A}}}$ and $\underline{\underline{\tilde{B}}}$ are both positive semi-definite, the generalized eigenvectors are orthogonal, that is, $\underline{\underline{\Phi}}^{-1} = \underline{\underline{\Phi}}^T$, and the generalized eigenvalues of $(\underline{\underline{\tilde{A}}}, \underline{\underline{\tilde{B}}})$ are nonnegative. The components of the root $\underline{\underline{\Lambda}} := \sqrt{\underline{\underline{\Lambda}}^2}$, which is diagonal as well, can be assumed to be nonnegative without loss of generality.

In the following, the emphasis is placed on positive definite $\underline{\underline{\tilde{A}}}$ and $\underline{\underline{\tilde{B}}}$, resulting in $\underline{\underline{\Lambda}}$ being regular. In this case, $\Delta\underline{\tilde{\gamma}}_1$ takes on the following form

$$\Delta\underline{\tilde{\gamma}}_1 = \underline{\underline{\Phi}}\ \cosh(\underline{\underline{\Lambda}}\ \tau)\ \underline{\alpha} + \underline{\underline{\Phi}}\ \sinh(\underline{\underline{\Lambda}}\ \tau)\ \underline{\beta} \tag{78}$$

$$= \sum_i \underline{\phi}_i\ \cosh(\lambda_i\tau)\ \alpha_i + \underline{\phi}_i\ \sinh(\lambda_i\tau)\ \beta_i. \tag{79}$$

The coefficient vectors $\underline{\alpha}$ and $\underline{\beta}$ can not be determined from Equation (71) and will be determined when incorporating the boundary conditions for the plastic slips.

The function $\Delta\underline{\tilde{\gamma}}_2$ is obtained from Equation (72) by choosing an ansatz of the same type similar to the forcing term

$$-\underline{\underline{\tilde{A}}}\ \Delta\underline{\tilde{\gamma}}_2 + \underline{\underline{\tilde{B}}}\ \Delta\underline{\tilde{\gamma}}_2'' = \underline{\underline{L}}\ \underline{\underline{A}}\ (\underline{\gamma}^{\mathrm{n}} - \underline{a}^{\mathrm{n}}) - \underline{\underline{L}}\ \underline{\underline{B}}\ \underline{\gamma}^{\mathrm{n}\prime\prime}. \tag{80}$$

Due to splitting the *constant* part from the forcing terms, we have

$$\underline{\gamma}^{\mathrm{n}} - \underline{a}^{\mathrm{n}} = \sum_{i=1}^{\infty} \underline{b}_i^{\mathrm{n}} \cosh(\Omega_i\tau) + \underline{d}_i^{\mathrm{n}} \sinh(\Omega_i\tau), \tag{81}$$

$$\underline{\gamma}^{\mathrm{n}\prime\prime} = \sum_{i=1}^{\infty} \Omega_i^2 \underline{b}_i^{\mathrm{n}} \cosh(\Omega_i\tau) + \Omega_i^2 \underline{d}_i^{\mathrm{n}} \sinh(\Omega_i\tau). \tag{82}$$

This motivates the following ansatz for $\Delta\tilde{\gamma}_2$

$$\Delta\underline{\tilde{\gamma}}_2 = \sum_i^{\infty} \underline{\underline{\Phi}}\ \underline{\Gamma}_i^{\mathrm{c}} \cosh(\Omega_i\tau) + \underline{\underline{\Phi}}\ \underline{\Gamma}_i^{\mathrm{s}} \sinh(\Omega_i\tau). \tag{83}$$

Inserting Equation (81) to (83) as well as Equation (75) all into Equation (80), and combining terms with the same frequency yields

$$\sum_{i}^{\infty}\left(\underline{\underline{\tilde{B}}}\,\underline{\underline{\Phi}}(-\underline{\underline{\Lambda}}^2+\Omega_i^2\underline{\underline{1}})\underline{\Gamma}_i^{\mathrm{c}}-(\underline{\underline{L}}\,\underline{\underline{A}}\;-\underline{\underline{L}}\,\underline{\underline{B}}\,\Omega_i^2)\underline{b}_i^{\mathrm{n}}\right)\cosh(\Omega_i\tau)$$
$$+\sum_{i}^{\infty}\left(\underline{\underline{\tilde{B}}}\,\underline{\underline{\Phi}}(-\underline{\underline{\Lambda}}^2+\Omega_i^2\underline{\underline{1}})\underline{\Gamma}_i^{\mathrm{s}}-(\underline{\underline{L}}\,\underline{\underline{A}}\;-\underline{\underline{L}}\,\underline{\underline{B}}\,\Omega_i^2)\underline{d}_i^{\mathrm{n}}\right)\sinh(\Omega_i\tau)=\underline{0}. \tag{84}$$

Due to the nonadditivity of the exponential map, in Equation (84) each term must vanish by its own, resulting in the decoupled equations

$$\underline{\underline{\tilde{B}}}\,\underline{\underline{\Phi}}(-\underline{\underline{\Lambda}}^2+\Omega_i^2\underline{\underline{1}})\underline{\Gamma}_i^{\mathrm{c}}-(\underline{\underline{L}}\,\underline{\underline{A}}\;-\underline{\underline{L}}\,\underline{\underline{B}}\,\Omega_i^2)\underline{b}_i^{\mathrm{n}}=\underline{0},\quad\forall i\in\mathbb{N}, \tag{85}$$

$$\underline{\underline{\tilde{B}}}\,\underline{\underline{\Phi}}(-\underline{\underline{\Lambda}}^2+\Omega_i^2\underline{\underline{1}})\underline{\Gamma}_i^{\mathrm{s}}-(\underline{\underline{L}}\,\underline{\underline{A}}\;-\underline{\underline{L}}\,\underline{\underline{B}}\,\Omega_i^2)\underline{d}_i^{\mathrm{n}}=\underline{0},\quad\forall i\in\mathbb{N}. \tag{86}$$

This gives explicit expressions of the unknowns $\underline{\Gamma}_i^{\mathrm{c}}$ and $\underline{\Gamma}_i^{\mathrm{s}}$

$$\underline{\Gamma}_i^{\mathrm{c}}=(\Omega_i^2\underline{\underline{1}}-\underline{\underline{\Lambda}}^2)^{-1}\underline{\underline{\Phi}}^T\underline{\underline{\tilde{B}}}^{-1}(\underline{\underline{L}}\,\underline{\underline{A}}\;-\underline{\underline{L}}\,\underline{\underline{B}}\,\Omega_i^2)\underline{b}_i^{\mathrm{n}},\quad\forall i\in\mathbb{N}, \tag{87}$$

$$\underline{\Gamma}_i^{\mathrm{s}}=(\Omega_i^2\underline{\underline{1}}-\underline{\underline{\Lambda}}^2)^{-1}\underline{\underline{\Phi}}^T\underline{\underline{\tilde{B}}}^{-1}(\underline{\underline{L}}\,\underline{\underline{A}}\;-\underline{\underline{L}}\,\underline{\underline{B}}\,\Omega_i^2)\underline{d}_i^{\mathrm{n}},\quad\forall i\in\mathbb{N}. \tag{88}$$

As mentioned above, this procedure assumes the regularity of $\underline{\underline{\tilde{B}}}$. This is equivalent to stating that the slip plane normal vectors of the active slip systems are not parallel to the lamination direction (cf. Appendix C). The back stress in those slip systems vanishes as shown later, such that we exclude them from the active set during the computation of $\Delta\underline{\tilde{\gamma}}_2$ which contributes to the back stress.

For the next step, we consider Equation (73). Again, we choose a constant ansatz corresponding to the type of the right-hand side. The integral terms of the already discussed solution increments and the solution vector of the previous time step can expressed analytically:

$$\langle\Delta\underline{\tilde{\gamma}}_1\rangle=\underline{\underline{\Phi}}\langle\cosh(\underline{\underline{\Lambda}}\tau)\rangle\underline{\alpha}, \tag{89}$$

$$\langle\Delta\underline{\tilde{\gamma}}_2\rangle=\sum_{i}^{\infty}\underline{\underline{\Phi}}\langle\cosh(\Omega_i\tau)\rangle\underline{\Gamma}_i^{\mathrm{c}}, \tag{90}$$

$$\langle\underline{\gamma}^{\mathrm{n}}\rangle=\underline{a}^{\mathrm{n}}+\sum_{i=1}^{\infty}\langle\cosh(\Omega_i\tau)\rangle\;\underline{b}_i^{\mathrm{n}}, \tag{91}$$

where the means of the hyperbolic sine vanish due to the symmetric integral bounds (Equation (52)) and the means of the hyperbolic cosine evaluate to:

$$\langle\cosh(\underline{\underline{\Lambda}}\tau)\rangle=\underline{\underline{\Lambda}}^{-1}\sinh(\underline{\underline{\Lambda}}), \tag{92}$$

$$\langle\cosh(\Omega_i\tau)\rangle=\frac{1}{\Omega_i}\sinh(\Omega_i). \tag{93}$$

Since $\Delta\underline{\tilde{\gamma}}_3$ is constant, its derivatives vanish and its mean is the function itself, that is,

$$\langle\Delta\underline{\tilde{\gamma}}_3\rangle=\Delta\underline{\tilde{\gamma}}_3, \tag{94}$$

$$\Delta\underline{\tilde{\gamma}}_3''=\underline{0} \tag{95}$$

such that $\Delta\underline{\tilde{\gamma}}_3$ can be computed from Equation (73) as

$$\Delta\underline{\tilde{\gamma}}_3=\underbrace{-(\underline{\underline{\tilde{A}}}+\underline{\underline{\tilde{C}}})^{-1}\underline{\underline{\tilde{C}}}\;\langle\underline{\underline{\Phi}}\langle\cosh(\underline{\underline{\Lambda}}\tau)\rangle\underline{\alpha}}_{\text{term 1}}\underbrace{-(\underline{\underline{\tilde{A}}}+\underline{\underline{\tilde{C}}})^{-1}\underline{\underline{\tilde{C}}}\;\langle\Delta\underline{\tilde{\gamma}}_2\rangle+\underline{\underline{L}}\,\underline{\underline{A}}\,\underline{a}^{\mathrm{n}}+\underline{\underline{L}}\,\underline{\underline{C}}\;\langle\underline{\gamma}^{\mathrm{n}}\rangle+\underline{\underline{L}}\;\underline{c}}_{\text{term 2}}. \tag{96}$$

Note, that $\Delta\underline{\tilde{\gamma}}_3$ is additively composed of two terms. The latter, term 2, involves only known terms, whereas the first term still has the unknown contribution from the homogeneous solution.

Now that all solution increments are computed, we can determine those unknowns $\underline{\alpha}$ and $\underline{\beta}$ using the boundary conditions at the interfaces. In the case of a microhard interface, we can determine the coefficients directly from the incremental solution

$$\Delta\underline{\tilde{\gamma}}(-1) = \underline{\underline{\Phi}}\cosh(\underline{\underline{\Lambda}})\underline{\alpha} - \underline{\underline{\Phi}}\sinh(\underline{\underline{\Lambda}})\underline{\beta} + \sum_i^{\infty}\underline{\underline{\Phi}}\,\underline{\Gamma}_i^{\mathrm{c}}\cosh(\Omega_i) - \sum_i^{\infty}\underline{\underline{\Phi}}\,\underline{\Gamma}_i^{\mathrm{s}}\sinh(\Omega_i) + \Delta\underline{\tilde{\gamma}}_3 = \underline{0}, \tag{97}$$

$$\Delta\underline{\gamma}(+1) = \underline{\underline{\Phi}}\cosh(\underline{\underline{\Lambda}})\underline{\alpha} + \underline{\underline{\Phi}}\sinh(\underline{\underline{\Lambda}})\underline{\beta} + \sum_i^{\infty}\underline{\underline{\Phi}}\,\underline{\Gamma}_i^{\mathrm{c}}\cosh(\Omega_i) + \sum_i^{\infty}\underline{\underline{\Phi}}\,\underline{\Gamma}_i^{\mathrm{s}}\sinh(\Omega_i) + \Delta\underline{\tilde{\gamma}}_3 = \underline{0}. \tag{98}$$

Note, that the assumption of microhard interfaces is not an inherent limitation of the proposed formulation. Instead the equations for determining the coefficient vectors $\underline{\alpha}$ and $\underline{\beta}$ from the general incremental solution need to be modified. Consider the exemplary case of microfree interfaces, with vanishing vector-valued stresses and consequently vanishing slip gradient. Here, Equations (97) and (98) are superseded by $\underline{\tilde{\gamma}}'(\pm 1) = \underline{0}$, leading to $\underline{\alpha} = \underline{\beta} = \underline{0}$, that is, a homogeneous slip distribution, which corresponds to the classical, nongradient enhanced solution. To account for more complex grain boundary behavior with slip system coupling and slip transmission [5], $\underline{\alpha}$ and $\underline{\beta}$ are obtainable from the grain boundary yield conditions which are introduced at the N interfaces of the N phase laminate.

Lastly, the coefficient vectors of the general solution (Equation (69)) are updated for the next simulation step according to

$$\underline{a}^{\mathrm{n+1}} = \underline{a}^{\mathrm{n}} + \underline{\underline{L}}^T\Delta\underline{\tilde{\gamma}}_3, \tag{99}$$

$$\underline{b}_j^{\mathrm{n+1}} = \underline{b}_j^{\mathrm{n}} + \underline{\underline{L}}^T\underline{\underline{\Phi}}\,\underline{\Gamma}_j^{\mathrm{c}} + \underset{ji}{\mathbb{A}}\,\underline{\underline{L}}^T\underline{\phi}_i\,\alpha_i, \tag{100}$$

$$\underline{d}_j^{\mathrm{n+1}} = \underline{d}_j^{\mathrm{n}} + \underline{\underline{L}}^T\underline{\underline{\Phi}}\,\underline{\Gamma}_j^{\mathrm{s}} + \underset{ji}{\mathbb{A}}\,\underline{\underline{L}}^T\underline{\phi}_i\,\beta_i. \tag{101}$$

Here, $\underset{ji}{\mathbb{A}}$ is an assembling operator which assigns the contribution of the homogeneous solution to its corresponding frequency and works as follows: If the eigenvalue is already in the set of eigenvalues, that is, $\lambda_k \in \{\Omega_j\}$, we add the contribution to its corresponding frequency. Otherwise we update the set of eigenvalues to include λ_k and initialize the corresponding vectors $\underline{b}_k^{\mathrm{n+1}} = \underline{\underline{L}}^T\underline{\phi}_k\alpha_k$ and $\underline{d}_k^{\mathrm{n+1}} = \underline{\underline{L}}^T\underline{\phi}_k\beta_k$.

In the described algorithm, all fields besides the plastic strain are assumed to be phase-wise constant, which allows for a compact notation of the incremental solution. Conceptually, the approach remains the same if we allow continuously varying fields in the phases, with the major difference being that the varying properties result in nonconstant coefficient matrices $\underline{\underline{A}}$, $\underline{\underline{B}}$ and $\underline{\underline{C}}$. However, as the linearity of the FIDE is preserved, a split of the solution vector can still be employed. The major challenge lies its computation which requires a scheme for solving ODE systems with nonconstant coefficients, which is beyond the scope of this work.

3 | NUMERICAL EXAMPLE: INFLUENCE OF THE LAMELLA WIDTHS

To investigate the influence of the lamella widths, we consider the following model problem of a laminate with two phases and $\boldsymbol{n} = \boldsymbol{e}_1$ subjected to a macroscopic shear deformation of the form $\bar{\varepsilon}(t) = \varepsilon(t)\,\boldsymbol{e}_1 \otimes^{\mathrm{s}} \boldsymbol{e}_2$. Each phase has one slip system with slip plane normals and slip directions of the form $\boldsymbol{n}_1^{\xi} = -\sin(\psi^{\xi})\boldsymbol{e}_1 + \cos(\psi^{\xi})\boldsymbol{e}_2$ and $\boldsymbol{d}_1^{\xi} = \cos(\psi^{\xi})\boldsymbol{e}_1 + \sin(\psi^{\xi})\boldsymbol{e}_2$, respectively. The chosen set of slip systems is *defective*, such that the macroscopic strain can, in general, not be realized by a linear combination of the Schmid tensors. This leads to an *apparent hardening* in the macroscopic stress-strain curve. In order to study the influence of the length in the hardening by itself, we align the systems with the macroscopic strain. To circumvent the edge case where $\underline{\underline{\tilde{A}}}$ becomes singular, we introduce a small misorientation of $\pm 1°$. The elastic constants of phase one resemble those of copper, while the constants for phase two are half of those to introduce elastic heterogeneity. The remaining material parameters are taken from [5]. All parameters are listed in Table 1 The widths of the lamellas are equal, $L^1 = L^2 = L$, and varied over a wide range in order to investigate their influence on the mechanical behavior.

TABLE 1 Material parameters.

Parameter	C_{1111}	C_{1122}	C_{1212}	τ_C	K_g	ψ
Phase 1	169.0 GPa	121.0 GPa	140.0 GPa	10.0 MPa	84.0 μN	+1°
Phase 2	84.5 GPa	60.5 GPa	70.0 GPa	20.0 MPa	84.0 μN	−1°

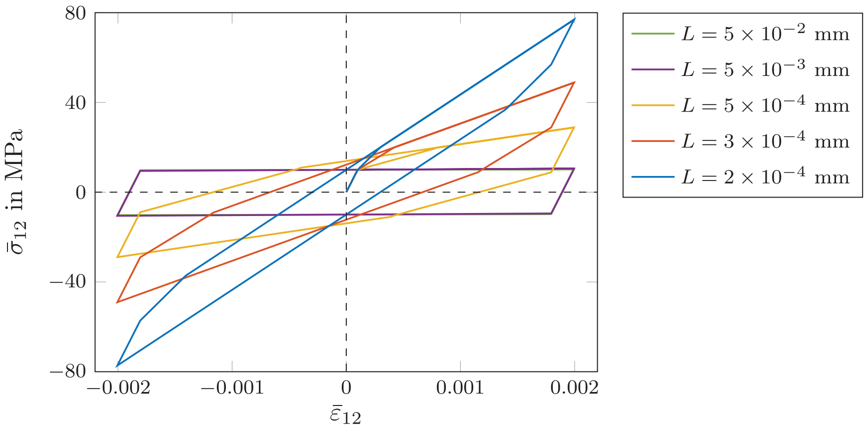

FIGURE 3 Comparison of the effective stress-strain curves of a periodic laminate with different phase widths under cyclic shear deformation.

Figure 3 shows the macroscopic stress response for cyclic shearing in the range $\bar{\varepsilon}_{12} \in [-0.002, 0.002]$ for different lengths. All stress-strain curves show a closed hysteresis with kinematic hardening. The kinematic hardening, shows a strong size-dependency and decreases with increasing lamella widths. For $L = 5 \times 10^{-2}$ mm and $L = 5 \times 10^{-3}$ mm, the stress strain curves coincide for all practical purposes, indicating that coarsening the lamellas beyond that has no further effect on the macroscopic behavior.

Generally, up to three states can be identified based on the slip system activity. In the stress-strain curves, the states correspond to sections with distinct slopes $\mathrm{d}\overline{\sigma}_{12}/\mathrm{d}\bar{\varepsilon}_{12}$:

- State I: No slip system is active and both phases deform elastically. This state occurs during the initial loading phase up until the onset of plastic deformation and immediately after strain rate reversals.
- State II: Once the yield conditions in the slip system with the lower critical shear stress is activated, the associated phase begins to yield, while the other phase continues to deform elastically. The effective stress increases further due to the back stress evolution induced by the inhomogeneous plastic deformation.
- State III: After sufficient back stress evolution in the weaker phase, the slip is activated as well, which is accompanied with an additional change of slope as both phases deform plastically.

The three states are shown in more detail in Figure 4 where the focus is set on the onset of plastification under monotonic loading while the lamella widths are varied between $L = 1 \times 10^{-4}$ mm and $L = 9 \times 10^{-4}$ mm.

For the chosen lamination direction and slip systems orientation, the resolved shear stresses in the slip systems are approximately the macroscopic shear stress, that is, $\tau^{\xi} \approx \overline{\sigma}_{12}$, such that the slip system activation can be directly deduced from the macroscopic stress response. For $\overline{\sigma}_{12} < 10$ MPa, the behavior is elastic and identical in all cases. At $\overline{\sigma}_{12} \approx 10$ MPa the first phase shows plastic deformation and stage II is entered with differing hardening behavior based on the phase widths. Once $\overline{\sigma}_{12} \approx 20$ MPa is reached, the second phase deforms plastically as well leading to a further decrease of the slope $\mathrm{d}\overline{\sigma}_{12}/\mathrm{d}\bar{\varepsilon}_{12}$. As the phase widths decrease, the macroscopic stress response converges towards the elastic behavior indicated by the dotted line in Figure 4. Note, that for a given strain amplitude in the case of cyclic loading or maximally reached strain in the case of monotonic loading, state III is only observed below a critical phase width, where the size-dependent kinematic hardening is sufficiently pronounced to activate the slip system with the higher critical shear stress.

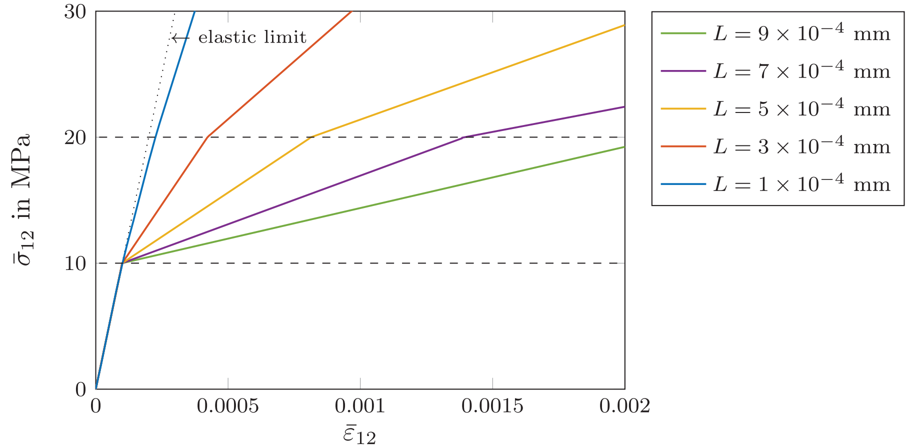

FIGURE 4 Comparison of the effective stress-strain curves of a periodic laminate with different phase widths under monotonic shear deformation.

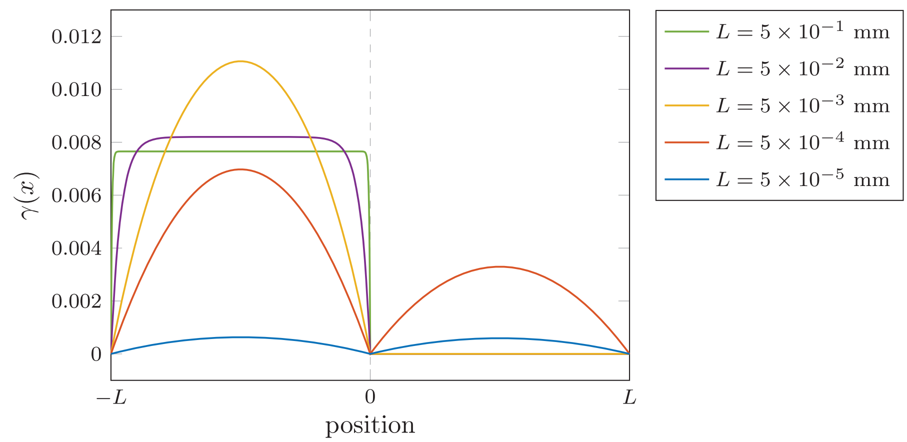

FIGURE 5 Comparison of the local distributions of the plastic slip for different phase widths L at $\bar{\varepsilon}_{12} = 0.002$.

Next, we investigate the influence of the lamella width on the local distributions by comparing the plastic slip at $\bar{\varepsilon}_{12} = 0.002$ which is depicted in Figure 5.

As mentioned before, stage III is not reached for lamella widths $L = 5 \times 10^{-3}$ mm and above, such that the phase with the higher critical shear stress remains elastic with no plastic deformation. Although the macroscopic behavior does not change for $L = 5 \times 10^{-3}$ mm and above, the local distribution of the plastic slip undergoes a transformation from a rectangular shape with a wide plateau ($L = 5 \times 10^{-1}$ mm) to a parabolic shape ($L = 5 \times 10^{-3}$ mm). At first, this mean-preserving redistribution of the plastic slip from the lamella boundaries towards the phase center leads to higher plastic slip at the phase center. Only upon further decrease of the lamella width, the plastic deformation is hindered, leading to a decrease of plastic slip, which is accompanied with an increase of the effective stress. This increase eventually leads to activation of the slip system with the higher critical shear stress ($L = 5 \times 10^{-4}$ mm). As the lamella width is even further decreased, the plastic slip converges towards zero, which is evident macroscopically with the convergence of the stress response towards the elastic limit.

4 | DIMENSIONLESS QUANTITY FOR THE SPATIAL DISTRIBUTION

In order to gain a more general understanding, we derive the underlying dimensionless quantity governing the spatial distribution of the plastic slip. For this, we consider a M-phase laminate with microhard interfaces each with one active slip system only, such that we must only differentiate between the different phases but not between multiple slip system within each phase. In this case, the plastic slips for $\xi = 1, \dots, M$ in each phase have the following spatial distribution

$$\gamma^{\xi}(\tau) \propto \left(1 - \frac{\cosh(\Omega^{\xi}\tau)}{\cosh(\Omega^{\xi})}\right). \tag{102}$$

The distribution is zero at the interfaces, that is, at $\tau = \pm 1$, and in between governed by the dimensionless parameters Ω^{ξ}, the roots of the generalized eigenvalues of the corresponding ODE. Due to the assumed single slip in each phase, Ω^{ξ} has the following closed form expression

$$\Omega^{\xi} = \sqrt{\frac{\boldsymbol{M}^{\xi} \cdot \mathbb{Z}^{\xi}[\boldsymbol{M}^{\xi}] + h^{\xi}}{K_{\mathrm{g}}^{\xi}\left(1 - (\boldsymbol{n}^{\xi} \cdot \boldsymbol{n})^2\right)\left(\frac{2}{L^{\xi}}\right)^2}}, \tag{103}$$

which depends on the local material properties, the orientation relative the lamination direction as well as the phase width. The expression is bounded by

$$\sqrt{\frac{h^{\xi}}{K_{\mathrm{g}}^{\xi}}}\frac{L^{\xi}}{2} \leq \Omega^{\xi} < \infty, \tag{104}$$

with the lower bound corresponding to slip systems with slip plane normals orthogonal to the lamination direction. The upper bound is, regardless of the (finite) phase width, given in slip systems with slip plane normals parallel to the lamination direction.

The qualitative shape of Equation (102) is bounded by a parabolic and a rectangular distribution for small and large Ω^{ξ}, respectively, such that the following holds

$$\lim_{\Omega^{\xi}\to 0} \gamma^{\xi}(\tau) \propto (1 - \tau^2) \tag{105}$$

$$\lim_{\Omega^{\xi}\to \infty} \gamma^{\xi}(\tau) \propto \operatorname{rect}\left(\frac{\tau}{2}\right). \tag{106}$$

Here, the rectangular function $\operatorname{rect}(\frac{\tau}{2})$ is used which is equal to one if $|\tau| < 1$ and zero everywhere else. From the distributions of γ^{ξ}, we can derive the qualitative distribution of the back stress, which is proportional to $\gamma^{\xi\prime\prime}$, as well as its bounds

$$\gamma^{\xi\prime\prime}(\tau) \propto \frac{\cosh(\Omega^{\xi}\tau)}{\cosh(\Omega^{\xi})}, \tag{107}$$

$$\lim_{\Omega^{\xi}\to 0} \gamma^{\xi\prime\prime}(\tau) \propto 1, \tag{108}$$

$$\lim_{\Omega^{\xi}\to \infty} \gamma^{\xi\prime\prime}(\tau) \propto 1 - \operatorname{rect}\left(\frac{\tau}{2}\right). \tag{109}$$

The qualitative distributions of the plastic slip and its second derivative are shown in Figure 6a,b. Note that the *bounds* only refer to the *normalized* shape, where the distributions are normalized by their maximum value, which occur at the phase center for the plastic slip and at the phase boundaries for the second derivative.

If the gradient contributions in the yield functions dominate, which is the case for $\Omega^{\xi} \to 0$, the plastic slip distribution has a parabolic shape whereas the back stress in that slip system is constant and nonzero. With increasing Ω^{ξ} the plastic slip distribution approaches the rectangular function as discussed. Additionally, the back stress, which initially is significant in the whole phase, becomes increasingly constricted to regions near the interface. The limit coincides with the classical laminate formulation where the fields inside the phases are constant and the back stress vanishes. Note that the bounding functions for $\Omega^{\xi} \to \infty$ are pointwise discontinuous, such that functions inside the phases are constant but different than the function at the interface.

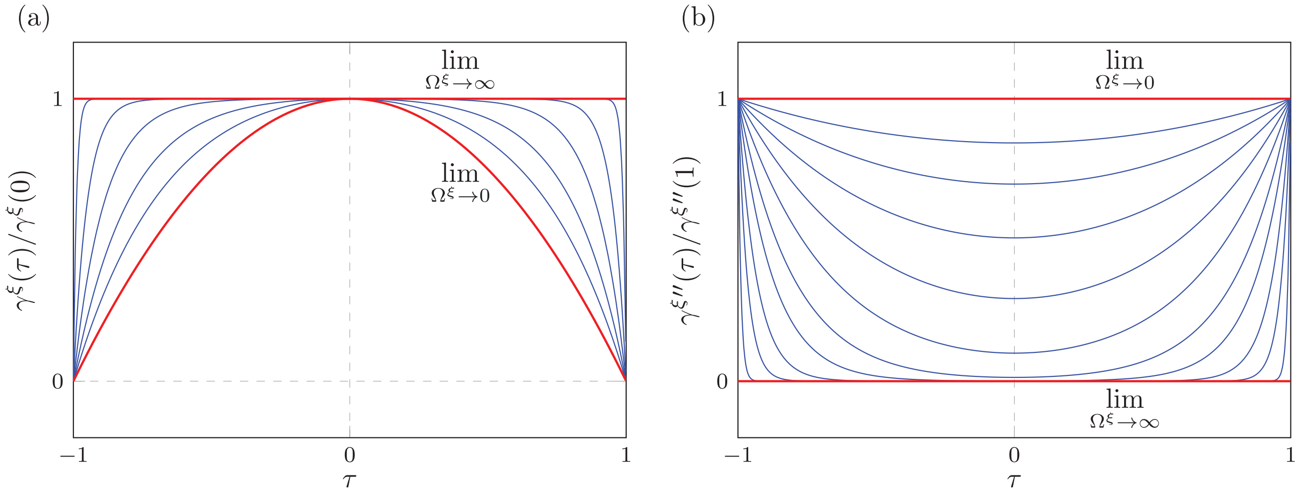

FIGURE 6 Qualitative distribution of the plastic slip (a) and its second derivative (b) for different values of Ω^ξ as well as the limiting cases $\Omega^\xi \to 0$ and $\Omega^\xi \to \infty$. The plots are normalized by their respective maximum value.

5 | SUMMARY AND CONCLUSIONS

In the present work, a gradient crystal plasticity framework has been combined with the exact strain localization of periodic laminates with multiple distinct phases in order to study the size-dependent mechanical behavior of lamellar materials. The new approach uses the concentration tensors to access the local strain and stress fields inside the laminate. This allows for a compact vectorized formulation of the yield functions governing the evolution of the plastic deformation. The approach has no constraints regarding the macroscopic strain rate and the elastic stiffness tensors of the phases as well as almost no constraints regarding the orientation of the slip systems. The latter is a direct consequence of using the planar slip gradient to model the size effect.

This generality opens up the possibility of investigating arbitrary, and therefore also more realistic, material systems. The main conclusions are summarized as follows:

- The emerging equations for determining the incremental plastic deformation are classified as a system of Fredholm integro-differential equations. For linear work hardening, the system can be solved analytically. In contrast to existing approaches, this new formulation allows for a general solution procedure using the direct computation method.
- The approach can model the kinematic hardening due to the back stress, induced by the inhomogeneous plastic deformation, under monotonic and cyclic loading. The numerical study shows a strong size-dependent kinematic hardening which decreases with increasing lamella widths.
- The kinematic hardening depends not only on the lamella widths, but also on the orientation of the active slip systems. Even for small lamella widths, the back stress, and therefore the kinematic hardening, vanishes in slip systems with slip plane normals parallel to the lamination direction.
- A dimensionless quantity governing the qualitative distribution of the plastic deformation and back stress is derived. For microhard interfaces, the qualitative distribution of the plastic slip is bounded by a parabolic shape in the case where the gradient contribution dominates, and by a rectangular shape, when the gradient contribution vanishes. The limiting distributions for the back stress are constant, but nonzero, and zero, respectively.

The generality of the presented framework makes it a suitable approach to be applied in multiscale simulations of lamellar materials, where the material behavior of the individual phases is not resolved numerically but, instead, the mechanical behavior is modeled using the proposed approach. To account for more complex grain boundary behavior, the existing framework can be extended by considering additional yield conditions at the interfaces.

AUTHOR CONTRIBUTIONS

Conceptualization, C.K.; Methodology, C.K.; Software, C.K.; Validation, C.K.; Formal Analysis, C.K.; Investigation, C.K.; Resources, T.B.; Data Curation, C.K.; Writing–Original Draft, C.K.; Writing–Review & Editing, C.K. and T.B.; Visualization, C.K.; Supervision, T.B.; Project Administration, T.B.; Funding Acquisition, T.B.

CONFLICT OF INTEREST STATEMENT

The authors declare no conflict of interest.

DATA AVAILABILITY STATEMENT

The data that support the findings of this study are available from the corresponding author upon reasonable request.

ACKNOWLEDGMENT

Open Access funding enabled and organized by Projekt DEAL.

REFERENCES

[1] M. Abatour and S. Forest, Strain gradient plasticity based on saturating variables, Euro. J. Mech. A/Solids **104** (2024), 105016. https://doi.org/10.1016/j.euromechsol.2023.105016.
[2] O. Aslan, N. M. Cordero, A. Gaubert, and S. Forest, Micromorphic approach to single crystal plasticity and damage, Int. J. Eng. Sci. **49** (2011), 1311–1325. https://doi.org/10.1016/j.ijengsci.2011.03.008.
[3] E. Bayerschen, M. Stricker, S. Wulfinghoff, D. Weygand, and T. Böhlke, Equivalent plastic strain gradient plasticity with grain boundary hardening and comparison to discrete dislocation dynamics, Proc. Royal Soc. A: Math. Phys. Eng. Sci. **471** (2015), 20150388. https://doi.org/10.1098/rspa.2015.0388.
[4] N. M. Cordero, A. Gaubert, S. Forest, E. Busso, F. Gallerneau, and S. Kruch, Size effects in generalised continuum crystal plasticity for two-phase laminates, J. Mech. Phys. Solids **58** (2010), 1963–1994. https://doi.org/10.1016/j.jmps.2010.06.012.
[5] H. Erdle and T. Böhlke, Analytical investigation of a grain boundary model that accounts for slip system coupling in gradient crystal plasticity frameworks, Proc. Royal Soc. A: Math. Phys. Eng. Sci. **479** (2023), 20220737. https://doi.org/10.1098/rspa.2022.0737.
[6] S. Forest, Micromorphic approach for gradient elasticity, Viscoplasticity, and damage, J. Eng. Mech. **135** (2009), 117–131. https://doi.org/10.1061/(ASCE)0733-9399(2009)135:3(117).
[7] S. Forest and N. Gueninchault, Inspection of free energy functions in gradient crystal plasticity, Acta Mech. Sinica **29** (2013), 763–772.
[8] S. Forest and R. Sedláček, Plastic slip distribution in two-phase laminate microstructures: Dislocation-based versus generalize, Philos. Mag. **83** (2003), 245–276. https://doi.org/10.1080/0141861021000022255.
[9] R. Glüge, Effective plastic properties of laminates made of isotropic elastic plastic materials, Compos. Struct. **149** (2016), 434–443. https://doi.org/10.1016/j.compstruct.2016.04.029.
[10] R. Glüge and J. Kalisch, The effective stiffness and stress concentrations of a multi-layer laminate, Compos. Struct. **111** (2014), 580–586. https://doi.org/10.1016/j.compstruct.2014.01.027.
[11] M. E. Gurtin, On the plasticity of single crystals: free energy, microforces, plastic-strain gradients, J. Mech. Phys. Solids **48** (2000), 989–1036. https://doi.org/10.1016/S0022-5096(99)00059-9.
[12] Q. C. He and Z. Q. Feng, Homogenization of layered elastoplastic composites: Theoretical results, Int. J. Non-Linear Mech. **47** (2012), 367–376. https://doi.org/10.1016/j.ijnonlinmec.2011.09.018.
[13] R. Hill, Interfacial operators in the mechanics of composite media, J. Mech. Phys. Solids **31** (1983), 347–357. https://doi.org/10.1016/0022-5096(83)90004-2.
[14] R. Lebensohn, H. Uhlenhut, C. Hartig, and H. Mecking, Plastic flow of y-TiAl-based polysynthetically twinned crystals: Micromechanical modeling and experimental validation, Acta Mater. **46** (1998), 4701–4709. https://doi.org/10.1016/S1359-6454(98)00132-3.
[15] H. Li, J. Wang, N. Deng, W. Y. Wang, R. Yuan, and J. Li, Eutectoid lamellar structure strengthened ultra-strong Al13Fe29Co29Ni29 high-entropy alloy, Mater. Sci. Eng. A **856** (2022a), 143934. https://doi.org/10.1016/j.msea.2022.143934.
[16] Y. Li, P. Shi, M. Wang, Y. Yang, Y. Wang, Y. Li, Y. Wen, W. Ren, N. Min, Y. Chen, Y. Guo, Z. Shen, T. Zheng, N. Liang, W. Lu, P. K. Liaw, Y. Zhong, and Y. Zhu, Unveiling microstructural origins of the balanced strength–ductility combination in eutectic high-entropy alloys at cryogenic temperatures, Mat. Res. Lett. **10** (2022b), 602–610. https://doi.org/10.1080/21663831.2022.2078169.
[17] C. Miehe and J. Schröder, A comparative study of stress update algorithms for rate-independent and rate-dependent crystal plasticity, Int. J. Numer. Methods Eng. **50** (2001), 273–298. https://doi.org/10.1002/1097-0207(20010120)50:2¡273::AID-NME17¿3.0.CO;2-Q.
[18] G. W. Milton, *Theory of composites*, Cambridge University Press, Cambridge, 2012.
[19] A. Molabahrami, Direct computation method for solving a general nonlinear Fredholm integro-differential equation under the mixed conditions: Degenerate and non-degenerate kernels, J. Comput. Appl. Math. **282** (2015), 34–43. https://doi.org/10.1016/j.cam.2014.12.025.
[20] A. Palomares-García, I. Sabirov, M. Pérez-Prado, and J. Molina-Aldareguia, Effect of nanoscale thick lamellae on the micromechanical response of a TiAl alloy, Scr. Mater. **139** (2017a), 17–21. https://doi.org/10.1016/j.scriptamat.2017.06.002.

[21] A. J. Palomares-García, M. T. Pérez-Prado, and J. M. Molina-Aldareguia, Effect of lamellar orientation on the strength and operating deformation mechanisms of fully lamellar TiAl alloys determined by micropillar compression, Acta Mater. **123** (2017b), 102–114. https://doi.org/10.1016/j.actamat.2016.10.034.
[22] A. Prahs and T. Böhlke, On interface conditions on a material singular surface, Contin. Mech. Thermodyn. **32** (2020), 1417–1434. https://doi.org/10.1007/s00161-019-00856-1.
[23] A. Schmitt, K. Kumar, A. Kauffmann, and M. Heilmaier, Microstructural evolution during creep of lamellar eutectoid and off-eutectoid FeAl/FeAl2 alloys, Intermetallics **107** (2019), 116–125. https://doi.org/10.1016/j.intermet.2019.01.015.
[24] A. Schmitt, K. Kumar, A. Kauffmann, X. Li, F. Stein, and M. Heilmaier, Creep of binary Fe-Al alloys with ultrafine lamellar microstructures, Intermetallics **90** (2017), 180–187. https://doi.org/10.1016/j.intermet.2017.07.016.
[25] J. Schnabel and S. Bargmann, Accessing Colony boundary strengthening of fully lamellar TiAl alloys via micromechanical Modeling, Materials **10** (2017), 896. https://doi.org/10.3390/ma10080896.
[26] J. E. Schnabel and I. Scheider, Crystal plasticity Modeling of creep in alloys with lamellar microstructures at the example of fully lamellar TiAl, Front. Mater. **7** (2021), 581187. https://doi.org/10.3389/fmats.2020.581187.
[27] J. Schröder and C. Miehe, Aspects of computational rate-independent crystal plasticity, Comput. Mater. Sci. **9** (1997), 168–176. https://doi.org/10.1016/S0927-0256(97)00072-4.
[28] R. Sedláček and S. Forest, Non-local plasticity at microscale: A dislocation-based and a Cosserat model, Phys. Status Solidi B **221** (2000), 583–596.
[29] M. Šilhavý, *The mechanics and thermodynamics of continuous media*, Springer Berlin Heidelberg, Berlin, Heidelberg, 1997. https://doi.org/10.1007/978-3-662-03389-0.
[30] W. Sun, Y. Wu, S. Yang, and C. Hutchinson, Advanced high strength steel (AHSS) development through chemical patterning of austenite, Scr. Mater. **146** (2018), 60–63. https://doi.org/10.1016/j.scriptamat.2017.11.007.
[31] L. Walpole, "*Elastic behavior of composite materials: Theoretical foundations*," *Advances in applied mechanics*, Academic Press, New York, 1981, pp. 169–242. https://doi.org/10.1016/s0065-2156(08)70332-6.0065-2156.
[32] S. Wulfinghoff, E. Bayerschen, and T. Böhlke, Conceptual difficulties in plasticity including the gradient of one scalar plastic field variable, PAMM **14** (2014), 317–318. https://doi.org/10.1002/pamm.201410146.
[33] S. Wulfinghoff, S. Forest, and T. Böhlke, Strain gradient plasticity modeling of the cyclic behavior of laminate microstructures, J. Mech. Phys. Solids **79** (2015), 1–20. https://doi.org/10.1016/j.jmps.2015.02.008.

How to cite this article: C. Klein and T. Böhlke, *Gradient Crystal Plasticity Modeling of Laminate Microstructures*, GAMM-Mitteilungen. **48** (2025), e70009. https://doi.org/10.1002/gamm.70009

APPENDIX A. DERIVATION OF LAMINATE LOCALIZATION

The constitutive relation for the stress and its inverse are given by the following affine functions

$$\boldsymbol{\sigma} = \mathbb{C}[\boldsymbol{\varepsilon} - \boldsymbol{\varepsilon}_{\mathrm{p}}], \tag{A1}$$

$$\boldsymbol{\varepsilon} = \mathbb{S}[\boldsymbol{\sigma}] + \boldsymbol{\varepsilon}_{\mathrm{p}}. \tag{A2}$$

Volume averaging the local stress and strain fields yields their macroscopic equivalents

$$\overline{\boldsymbol{\sigma}} = \langle \boldsymbol{\sigma} \rangle, \tag{A3}$$

$$\overline{\boldsymbol{\varepsilon}} = \langle \boldsymbol{\varepsilon} \rangle. \tag{A4}$$

The equilibrium and compatibility are expressed using the projectors

$$\boldsymbol{\sigma} = \langle \boldsymbol{\sigma} \rangle + \mathbb{P}_{\parallel}[\boldsymbol{\sigma} - \langle \boldsymbol{\sigma} \rangle], \tag{A5}$$

$$\boldsymbol{\varepsilon} = \langle \boldsymbol{\varepsilon} \rangle + \mathbb{P}_{\perp}[\boldsymbol{\varepsilon} - \langle \boldsymbol{\varepsilon} \rangle]. \tag{A6}$$

In order to derive the localization relations, we are interested in closed form expressions for the fluctuations in terms of macroscopic quantities. This is achieved in the following way.

Inserting Equation (A5) into Equation (A1) and Equation (A6) into Equation (A2) yields

$$\boldsymbol{\sigma} = \mathbb{C}[\overline{\boldsymbol{\varepsilon}}] + \mathbb{C}\mathbb{P}_{\perp}[\boldsymbol{\varepsilon} - \overline{\boldsymbol{\varepsilon}}] - \mathbb{C}[\boldsymbol{\varepsilon}_{\mathrm{p}}], \tag{A7}$$

$$\boldsymbol{\varepsilon} = \mathbb{S}[\overline{\boldsymbol{\sigma}}] + \mathbb{S}\mathbb{P}_{\parallel}[\boldsymbol{\sigma} - \overline{\boldsymbol{\sigma}}] + \boldsymbol{\varepsilon}_{\mathrm{p}}. \tag{A8}$$

Rearranging and projecting Equation (A7) onto $\mathcal{V}_{\perp}$ and Equation (A8) onto $\mathcal{V}_{\parallel}$ yields

$$\mathbb{P}_{\perp}\mathbb{C}\mathbb{P}_{\perp}[\boldsymbol{\varepsilon} - \overline{\boldsymbol{\varepsilon}}] = \mathbb{P}_{\perp}[\overline{\boldsymbol{\sigma}}] - \mathbb{P}_{\perp}\mathbb{C}[\overline{\boldsymbol{\varepsilon}}] + \mathbb{P}_{\perp}\mathbb{C}[\boldsymbol{\varepsilon}_{\mathrm{p}}], \tag{A9}$$

$$\mathbb{P}_{\parallel}\mathbb{S}\mathbb{P}_{\parallel}[\boldsymbol{\sigma} - \overline{\boldsymbol{\sigma}}] = \mathbb{P}_{\parallel}[\overline{\boldsymbol{\varepsilon}}] - \mathbb{P}_{\parallel}\mathbb{S}[\overline{\boldsymbol{\sigma}}] - \mathbb{P}_{\parallel}[\boldsymbol{\varepsilon}_{\mathrm{p}}], \tag{A10}$$

where we use $\mathbb{P}_{\perp}[\boldsymbol{\sigma}] = \mathbb{P}_{\perp}[\overline{\boldsymbol{\sigma}}]$ and $\mathbb{P}_{\parallel}[\boldsymbol{\varepsilon}] = \mathbb{P}_{\parallel}[\overline{\boldsymbol{\varepsilon}}]$. Next, we define the auxiliary tensors $\mathbb{K}$ and $\mathbb{Z}$ as inverses of the projections of $\mathbb{C}$ and $\mathbb{S}$ onto $\mathcal{V}_{\perp}$ and $\mathcal{V}_{\parallel}$ with respect to those subspaces, that is,

$$\mathbb{K} := (\mathbb{P}_{\perp}\mathbb{C}\mathbb{P}_{\perp})^{\dagger}, \text{ s.t. } \mathbb{K}(\mathbb{P}_{\perp}\mathbb{C}\mathbb{P}_{\perp}) = \mathbb{P}_{\perp}, \tag{A11}$$

$$\mathbb{Z} := (\mathbb{P}_{\parallel}\mathbb{S}\mathbb{P}_{\parallel})^{\dagger}, \text{ s.t. } \mathbb{Z}(\mathbb{P}_{\parallel}\mathbb{S}\mathbb{P}_{\parallel}) = \mathbb{P}_{\parallel}. \tag{A12}$$

Note that the usual tensor representation of linear maps $Sym \to Sym$ as 6×6 matrices results in singular matrices, leading to problems during the inversion. This can be circumvented by calculating the inverses on their corresponding subspaces. With respect to the lower dimensional bases, the expressions $\mathbb{P}_{\perp}\mathbb{C}\mathbb{P}_{\perp}$ and $\mathbb{P}_{\parallel}\mathbb{S}\mathbb{P}_{\parallel}$ result in regular 3×3 matrices. Once inverted by means of conventional matrix inversion, the corresponding representations as singular 6×6 matrices are found using the projectors $\mathcal{V}_{\perp} \to Sym$ and $\mathcal{V}_{\parallel} \to Sym$. Alternatively, the same is achieved by using the Moore-Penrose inverse. Using either approach, we can solve for the stress and strain fluctuations

$$\mathbb{P}_{\perp}[\boldsymbol{\varepsilon} - \overline{\boldsymbol{\varepsilon}}] = \mathbb{K}[\overline{\boldsymbol{\sigma}}] - \mathbb{K}\mathbb{C}[\overline{\boldsymbol{\varepsilon}}] + \mathbb{K}\mathbb{C}[\boldsymbol{\varepsilon}_{\mathrm{p}}], \tag{A13}$$

$$\mathbb{P}_{\parallel}[\boldsymbol{\sigma} - \overline{\boldsymbol{\sigma}}] = \mathbb{Z}[\overline{\boldsymbol{\varepsilon}}] - \mathbb{Z}\mathbb{S}[\overline{\boldsymbol{\sigma}}] - \mathbb{Z}[\boldsymbol{\varepsilon}_{\mathrm{p}}]. \tag{A14}$$

Additionally, we average Equation (A13) and Equation (A14) and make use of the subspace inverses to find

$$\mathbb{P}_{\perp}[\overline{\boldsymbol{\sigma}}] = \langle\mathbb{K}\rangle^{\dagger}\langle\mathbb{K}\mathbb{C}\rangle[\overline{\boldsymbol{\varepsilon}}] - \langle\mathbb{K}\rangle^{\dagger}\langle\mathbb{K}\mathbb{C}[\boldsymbol{\varepsilon}_{\mathrm{p}}]\rangle, \tag{A15}$$

$$\mathbb{P}_{\parallel}[\overline{\boldsymbol{\varepsilon}}] = \langle\mathbb{Z}\rangle^{\dagger}\langle\mathbb{Z}\mathbb{S}\rangle[\overline{\boldsymbol{\sigma}}] + \langle\mathbb{Z}\rangle^{\dagger}\langle\mathbb{Z}[\boldsymbol{\varepsilon}_{\mathrm{p}}]\rangle. \tag{A16}$$

Putting these results together, that is, inserting Equation (A15) and Equation (A14) into Equation (A5) and inserting Equation (A16) and Equation (A13) into Equation (A6) results in

$$\boldsymbol{\varepsilon} = \overline{\boldsymbol{\varepsilon}} + \mathbb{P}_{\perp}[\boldsymbol{\varepsilon} - \overline{\boldsymbol{\varepsilon}}] = (\mathbb{I}^{\mathrm{S}} - \mathbb{K}\mathbb{C})[\overline{\boldsymbol{\varepsilon}}] + \mathbb{K}\langle\mathbb{K}\rangle^{\dagger}\langle\mathbb{K}\mathbb{C}\rangle[\overline{\boldsymbol{\varepsilon}}] - \langle\mathbb{K}\rangle^{\dagger}\langle\mathbb{K}\mathbb{C}[\boldsymbol{\varepsilon}_{\mathrm{p}}]\rangle + \mathbb{K}\mathbb{C}[\boldsymbol{\varepsilon}_{\mathrm{p}}], \tag{A17}$$

$$\boldsymbol{\sigma} = \overline{\boldsymbol{\sigma}} + \mathbb{P}_{\parallel}[\boldsymbol{\sigma} - \overline{\boldsymbol{\sigma}}] = (\mathbb{I}^{\mathrm{S}} - \mathbb{Z}\mathbb{S})[\overline{\boldsymbol{\sigma}}] + \mathbb{Z}\langle\mathbb{Z}\rangle^{\dagger}\langle\mathbb{Z}\mathbb{S}\rangle[\overline{\boldsymbol{\sigma}}] + \langle\mathbb{Z}\rangle^{\dagger}\langle\mathbb{Z}[\boldsymbol{\varepsilon}_{\mathrm{p}}]\rangle - \mathbb{Z}[\boldsymbol{\varepsilon}_{\mathrm{p}}]. \tag{A18}$$

For a shorter expression, we make use of the identity

$$\mathbb{K}\mathbb{C} + \mathbb{S}\mathbb{Z} = \mathbb{C}\mathbb{K} + \mathbb{Z}\mathbb{S} = \mathbb{I}^{\mathrm{S}} \tag{A19}$$

to arrive at the final expression for the localization relationship

$$\boldsymbol{\varepsilon} = (\mathbb{S}\mathbb{Z} + \mathbb{K}\langle\mathbb{K}\rangle^{\dagger}\langle\mathbb{K}\mathbb{C}\rangle)[\overline{\boldsymbol{\varepsilon}}] + \mathbb{K}\mathbb{C}[\boldsymbol{\varepsilon}_{\mathrm{p}}] - \mathbb{K}\langle\mathbb{K}\rangle^{\dagger}\langle\mathbb{K}\mathbb{C}[\boldsymbol{\varepsilon}_{\mathrm{p}}]\rangle, \tag{A20}$$

$$\boldsymbol{\sigma} = (\mathbb{C}\mathbb{K} + \mathbb{Z}\langle\mathbb{Z}\rangle^{\dagger}\langle\mathbb{Z}\mathbb{S}\rangle)[\overline{\boldsymbol{\sigma}}] - \mathbb{Z}[\boldsymbol{\varepsilon}_{\mathrm{p}}] + \mathbb{Z}\langle\mathbb{Z}\rangle^{\dagger}\langle\mathbb{Z}[\boldsymbol{\varepsilon}_{\mathrm{p}}]\rangle. \tag{A21}$$

Comparing the coefficients with equations Equation (29) and Equation (30) allows the identification of all localization and fluctuation tensors given in [12].

APPENDIX B. EXTENSION DIFFERENT HARDENING MECHANISMS

The extension to account for different hardening mechanism is straight-forward. In order to preserve the linearity of the Fredholm integro-differential equation, only hardening functions of the following form are investigated

$$\tau^{\xi}_{\mathrm{C},\alpha} = \tau^{\xi}_{\mathrm{C0},\alpha} + \sum_{\beta=1}^{N_{\xi}} h^{\xi}_{\alpha\beta}\ \gamma^{\xi}_{\mathrm{ac},\beta}, \tag{B1}$$

where $\tau^{\xi}_{\mathrm{C0},\alpha}$ is the initial critical shear stress and $h^{\xi}_{\alpha\beta}$ are the hardening moduli. If all slip system are of the same type, we can choose a linear combination of isotropic latent hardening and self-hardening, with hardening moduli h^{ξ}_{l} and h^{ξ}_{s}, in the form

$$h^{\xi}_{\alpha\beta} = h^{\xi}_{\mathrm{s}} + h^{\xi}_{\mathrm{l}}\ \delta_{\alpha\beta}. \tag{B2}$$

Independent of the explicit form of the hardening moduli, Equation (B1) can be assembled into matrix vector notation yielding the hardening matrix $\underline{\underline{H}}$

$$\underline{\underline{H}} = \text{block-diag}(\underline{\underline{H}}^{1}, \underline{\underline{H}}^{2}, \cdots, \underline{\underline{H}}^{M}), \qquad H^{\xi}_{\alpha\beta} = h^{\xi}_{\alpha\beta}, \tag{B3}$$

which modifies the vectorized yield conditions to be

$$\underline{\varphi} = -(\underline{\underline{A}} + \underline{\underline{H}})\ \underline{\gamma} + \underline{\underline{B}}\ \underline{\gamma}'' - \underline{\underline{C}}\ \langle \underline{\gamma} \rangle - \underline{c}. \tag{B4}$$

The subsequent solution procedure using the direct computation method, described in Section 2.6, is not affected. In contrast, the extension to nonlinear hardening is not straight-forward. If the full nonlinear relationship between the critical shear stress and the accumulated plastic slip is considered, the FIDE becomes nonlinear, which prohibits the incremental solution using an hyperbolic series. If we instead approximate the nonlinear relationship incrementally by a linear one, the hardening matrix becomes spatially nonconstant due to different hardening moduli at different positions, leading to a nonconstant coefficient matrix $\underline{\underline{H}}(\tau)$ in the FIDE. This also prohibits the solution using the proposed method.

APPENDIX C. PROPERTIES OF THE RELEVANT MATRICES

Here, we show that the active set matrices $\underline{\underline{\tilde{A}}}$, $\underline{\underline{\tilde{H}}}$, $\underline{\underline{\tilde{B}}}$ and $\underline{\underline{\tilde{C}}}$, which are the equivalents of $\underline{\underline{A}}$, $\underline{\underline{H}}$, $\underline{\underline{B}}$ and $\underline{\underline{C}}$ when defined for the active set only, are positive semi-definite (p.s.d.) and under which conditions they even are positive-definite (p.d.). The active set matrices are obtained by "deleting" the rows and columns associated with *inactive* slip systems. Since $\underline{\underline{\tilde{A}}}$, $\underline{\underline{\tilde{H}}}$, $\underline{\underline{\tilde{B}}}$ have a block diagonal structure, it is sufficient to show that its submatrices $\underline{\underline{\tilde{A}}}^{\xi}$, $\underline{\underline{\tilde{H}}}^{\xi}$, $\underline{\underline{\tilde{B}}}^{\xi}$ are p.s.d., which will be done in the following:

For $\underline{\underline{\tilde{A}}}$ to be p.s.d, the following has to hold:

$$\underline{x}^{T}\ \underline{\underline{\tilde{A}}}^{\xi}\ \underline{x} \equiv \underbrace{\sum_{\alpha} (\tilde{\boldsymbol{M}}^{\xi}_{\alpha} x_{\alpha})}_{:=\boldsymbol{E}} \cdot \mathbb{Z}^{\xi}[\underbrace{\sum_{\beta} \tilde{\boldsymbol{M}}^{\xi}_{\beta} x_{\beta}}_{:=\boldsymbol{E}}] \geq 0, \forall \underline{x}. \tag{C1}$$

Due to semi-positive-definiteness of $\mathbb{Z}$, we can directly conclude that $\underline{\underline{\tilde{A}}}$ is always at least s.p.d as well. Furthermore, we can specify when the matrix is even p.d. We see directly that Equation (C1) equates to 0, if at least one of the following two conditions is met. Either the active slip systems are redundant, that is, nontrivial linear combinations of the Schmid tensors exist that equate to zero, such that $\boldsymbol{E} = \boldsymbol{0}$ for $\underline{x} \neq 0$. Alternatively, $\boldsymbol{E}$ itself is an eigentensor of $\mathbb{Z}$ corresponding to a zero eigenvalue, implying $\mathbb{Z}[\boldsymbol{E}] = \boldsymbol{0}$, which is fulfilled if $\boldsymbol{E} \in \mathcal{V}_{\perp}$.

In order to have a unique active set, we wish $\underline{\underline{\tilde{H}}}^{\xi}$ to be p.d., such that the following has to hold

$$\underline{x}^T \ \underline{\underline{\tilde{H}}}^{\xi} \ \underline{x} \equiv \sum_{\alpha,\beta} x_\alpha \tilde{h}^{\xi}_{\alpha\beta} x_\beta > 0, \forall \underline{x} \neq \underline{0}. \tag{C2}$$

With the typical split into self hardening and latent hardening and using the coefficients of the one-matrix, that is, $J_{\alpha\beta} = 1$, it follows that

$$\begin{aligned} \sum_{\alpha,\beta} x_\alpha \tilde{h}^{\xi}_{\alpha\beta} x_\beta &= \sum_{\alpha,\beta} x_\alpha \left((h^{\xi}_{\mathrm{s}} - h^{\xi}_{\mathrm{l}})\delta_{\alpha\beta} + h^{\xi}_{\mathrm{l}} J_{\alpha\beta} \right) x_\beta \\ &= (h^{\xi}_{\mathrm{s}} - h^{\xi}_{\mathrm{l}}) \underbrace{\left(\sum_{\alpha} x_\alpha x_\alpha \right)}_{>0} + h^{\xi}_{\mathrm{l}} \underbrace{\left(\sum_{\alpha} x_\alpha \right)^2}_{\geq 0} > 0, \forall \underline{x} \neq \underline{0}. \end{aligned} \tag{C3}$$

For nonnegative coefficients and $h^{\xi}_{\mathrm{s}} > h^{\xi}_{\mathrm{l}}$, the inequality is always fulfilled as seen above and $\underline{\underline{\tilde{H}}}$ is p.d.

Although, $\underline{\underline{B}}$ is block-diagonal, the projection onto the active set results in a diagonal $\underline{\underline{\tilde{B}}}$, since only one slip direction per slip system can be active at once. Due to the diagonal structure of $\underline{\underline{\tilde{B}}}$, we can inspect the matrix components on the diagonal

$$\tilde{B}^{\xi}_{\alpha\alpha} = K^{\xi}_{\mathrm{g},\alpha} \left(1 - (\boldsymbol{n}^{\xi}_{\alpha} \cdot \boldsymbol{n})^2 \right) \left(\frac{2}{L^{\xi}} \right)^2. \tag{C4}$$

If all entries are nonnegative, $\underline{\underline{\tilde{B}}}$ is p.s.d. and if all entries are positive, $\underline{\underline{\tilde{B}}}$ is p.d. For finite lengths $L^{\xi} < \infty$ and kinematic *hardening*, that is, $K^{\xi}_{\mathrm{g},\alpha} > 0$, the components vanish only if $\boldsymbol{n}^{\xi}_{\alpha} \cdot \boldsymbol{n} = 1$, which is the case if the slip plane normal is parallel to the lamination direction.

Showing the properties of $\underline{\underline{\tilde{C}}}$ requires more work, as it is not symmetric in the used formulation, which naturally arises when inserting the strain localization into the yield functions. Although, the matrices on its diagonal are symmetric, that is, $C^{\xi\xi}_{\alpha\beta} = C^{\xi\xi}_{\beta\alpha}$, its off-diagonal entries only fulfill $c^{\xi} C^{\xi\eta}_{\alpha\beta} = c^{\eta} C^{\eta\xi}_{\beta\alpha}$. To remedy this, we multiply the ξth block row of the FIDE system of the active set (compare Equation (67)) by the volume fraction of its corresponding phase c^{ξ}. This changes neither the systems solution nor changes any of the statements about $\underline{\underline{\tilde{A}}}$, $\underline{\underline{\tilde{H}}}$, $\underline{\underline{\tilde{B}}}$ as they have a block-diagonal structure, so every block is simply multiplied by a positive scalar. It does however modify $\underline{\underline{\tilde{C}}}$ into $\underline{\underline{\hat{C}}}$ which is now symmetric

$$\underline{\underline{\hat{C}}} = \begin{bmatrix} \underline{\underline{\hat{C}}}^{11} & \underline{\underline{\hat{C}}}^{12} & \cdots & \underline{\underline{\hat{C}}}^{1M} \\ \underline{\underline{\hat{C}}}^{21} & \underline{\underline{\hat{C}}}^{22} & \cdots & \underline{\underline{\hat{C}}}^{2M} \\ \vdots & \vdots & \ddots & \vdots \\ \underline{\underline{\hat{C}}}^{M1} & \underline{\underline{\hat{C}}}^{M2} & \cdots & \underline{\underline{\hat{C}}}^{MM} \end{bmatrix} = \begin{bmatrix} c^1 \underline{\underline{\tilde{C}}}^{11} & c^1 \underline{\underline{\tilde{C}}}^{12} & \cdots & c^1 \underline{\underline{\tilde{C}}}^{1M} \\ c^2 \underline{\underline{\tilde{C}}}^{21} & c^2 \underline{\underline{\tilde{C}}}^{22} & \cdots & c^2 \underline{\underline{\tilde{C}}}^{2M} \\ \vdots & \vdots & \ddots & \vdots \\ c^M \underline{\underline{\tilde{C}}}^{M1} & c^M \underline{\underline{\tilde{C}}}^{M2} & \cdots & c^M \underline{\underline{\tilde{C}}}^{MM} \end{bmatrix}. \tag{C5}$$

From its the components which are given by

$$\hat{C}^{\xi\eta}_{\alpha\beta} = c^{\xi} \tilde{\boldsymbol{M}}^{\xi}_{\alpha} \cdot \mathbb{C}^{\xi} \mathbb{K}^{\xi} \langle \mathbb{K} \rangle^{-1} \mathbb{K}^{\eta} \mathbb{C}^{\eta} [\tilde{\boldsymbol{M}}^{\eta}_{\beta}] c^{\eta}, \tag{C6}$$

we can see that $\hat{C}^{\xi\eta}_{\alpha\beta} = \hat{C}^{\eta\xi}_{\beta\alpha}$ does indeed hold. Next we introduce auxiliary tensors $\boldsymbol{G}^{\xi}_{\alpha}$ for each slip system α in each phase ξ giving us a shorter notation of $\hat{C}^{\xi\eta}_{\alpha\beta}$ via

$$\hat{C}^{\xi\eta}_{\alpha\beta} = \boldsymbol{G}^{\xi}_{\alpha} \cdot \langle \mathbb{K} \rangle^{-1} [\boldsymbol{G}^{\eta}_{\beta}], \qquad \boldsymbol{G}^{\xi}_{\alpha} = c^{\xi} \mathbb{K}^{\xi} \mathbb{C}^{\xi} [\boldsymbol{M}^{\xi}_{\alpha}]. \tag{C7}$$

The condition for positive definiteness of C reads

$$\underline{\hat{x}}^T\ \underline{\underline{\hat{C}}}\ \underline{\hat{x}} = \sum_{\xi,\alpha,\eta,\beta} x_\alpha^\xi \hat{C}_{\alpha\beta}^{\xi\eta} x_\beta^\eta = \underbrace{\left(\sum_{\xi,\alpha} x_\alpha^\xi \boldsymbol{G}_\alpha^\xi\right)}_{:=\boldsymbol{F}} \cdot <\mathbb{K}>^{-1} \left[\underbrace{\left(\sum_{\eta,\beta} \boldsymbol{G}_\beta^\eta x_\beta^\eta\right)}_{:=\boldsymbol{F}}\right] \geq 0, \forall \underline{x} \tag{C8}$$

Analogously, we can directly conclude that $\underline{\underline{\hat{C}}}$ is at least p.s.d. since $\langle\mathbb{K}\rangle^{-1}$ is p.s.d. as well. Similarly to before, we can also conclude, that $\underline{\underline{\hat{C}}}$ is p.d. if one of the following is true. Either a nontrivial linear combination of $\boldsymbol{G}_\alpha^\xi$ exists, resulting in $\boldsymbol{F} = \boldsymbol{0}$ for $\boldsymbol{x} \neq \underline{0}$, or $\boldsymbol{F}$ is an eigentensor of $\langle\mathbb{K}\rangle^{-1}$, which is the case if $\boldsymbol{F} \in \mathcal{V}_{\|}$. However, an intuitive mechanical interpretation is not obvious.

The consequences of this are clear: Since $\underline{\underline{\tilde{H}}}$ is p.d., its sum with any p.s.d. matrix such as $\underline{\underline{\tilde{A}}}$, $\underline{\underline{\tilde{C}}}$ or both is always p.d. and, thus, invertible. Furthermore, since $\underline{\underline{\tilde{A}}} + \underline{\underline{\tilde{H}}}$ is p.d. and $\underline{\underline{\tilde{B}}}$ is almost always p.d. (except when slip plane normals are parallel to the lamination direction), the generalized eigenvalues $\underline{\underline{\Lambda}}^2$ are always positive and almost always nonnegative and, consequently, $\underline{\underline{\Lambda}}$ is always real.